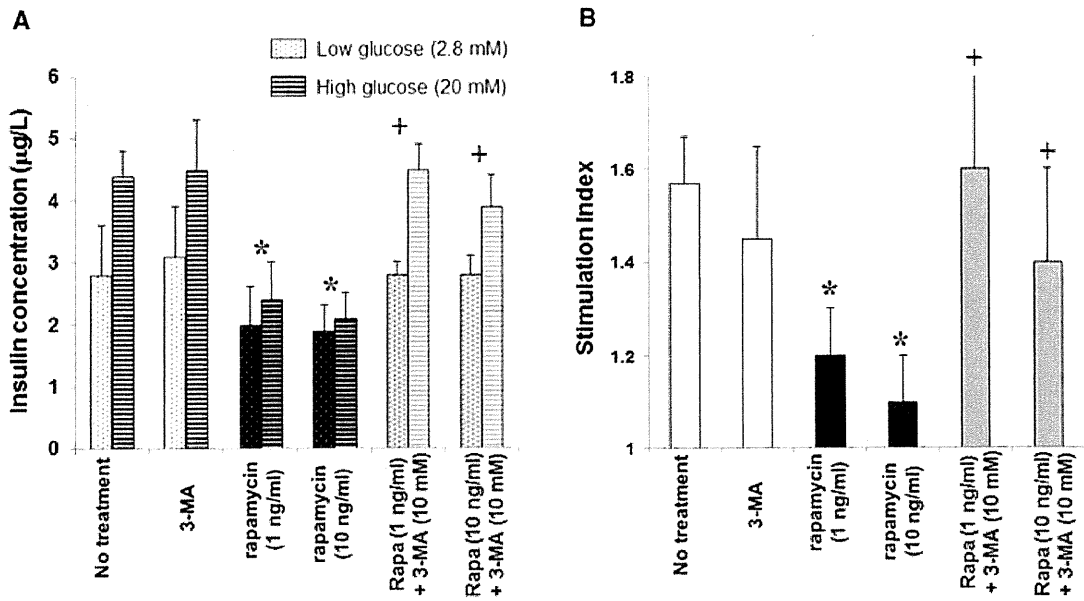

Figure 5: *In vitro* assessment of the effect of rapamycin on insulin production from islets. Production of insulin was assessed by static glucose challenge and the results expressed as both (A) blood insulin concentration and (B) stimulation index (SI). Data are mean ± SD of five independent islet preparations. *$p < 0.05$, compared with the control; $^{+}p < 0.05$, compared with rapamycin alone.

(1 ng/mL of rapamycin, 62.4 ± 6.7%; 10 ng/mL of rapamycin, 52.1 ± 6.1%; compared with the control, $p < 0.05$), and significantly increased the percentage of 7-AAD-positive cells (1 ng/mL of rapamycin, 17.7 ± 7.6%; 10 ng/mL of rapamycin, 18.7 ± 6.7%; compared with the control islets, $p < 0.05$). The addition of 3-MA to rapamycin-treated islets ameliorated the effects of the latter on the percentages of both viable and dead cells (Figures 4A and B). Taken together, these data suggest that rapamycin-induced overinduction of autophagy negatively affects islet viability and mitochondrial integrity, and that these effects are blocked by 3-MA.

Rapamycin reduces islet insulin production

Islet insulin potency was assessed by static glucose challenge *in vitro*. In control islets, insulin was secreted at 4.4–4.5 μg/L under high glucose medium (Figure 5A). In contrast, insulin secretion under high glucose medium was significantly inhibited in rapamycin-treated islets and treatment with rapamycin elicited approximately 45–53% reduction in insulin concentration (Figure 5A). We also analyzed islets' insulin production using the SI. The SI of untreated control islets was 1.57 ± 0.13 (Figure 5B). 3-MA did not have a significant effect on insulin production compared with the control islets. However, rapamycin significantly reduced the SI (1 ng/mL of rapamycin, 1.20 ± 0.1; 10 ng/mL of rapamycin, 1.11 ± 0.12; $p < 0.05$, each, compared with the control islets). The addition of 3-MA to rapamycin-treated islets markedly improved both insulin production and SI. Especially, insulin production showed complete recovery in islet treated with 1 ng/mL of rapamycin and 10 mM of 3-MA (Figures 5A and B). These results indicate that rapamycin elicits not only overinduction of autophagy but also reduction of both islet viability and *in vitro* insulin function.

Effect of nutrient starvation on autophagy in GFP-LC3 transgenic mice

To confirm the beneficial effects of 3-MA on induction of autophagy in the intact animal, we used GFP-LC3 transgenic mice and examined autophagy in 3-MA-treated transgenic mice under starvation. In the control GFP-LC3 transgenic mice, few GFP-LC3 dots were observed in pancreatic acinar cells and such dots were relatively small. In the pancreatic islets, no GFP dots were detected and these islets were clearly stained for insulin (top panels, Figure 6). The GFP-LC3 structures appeared 24 h after starvation as large cup-shaped structures in both islet and acinar cells. To validate these findings, we examined both muscle (as an example of nonessential tissue) and brain (as an essential tissue) tissues by fluorescence microscopy. As shown in Figure 7(A), no GFP dots were observed in the extensor digitorum longus muscles before starvation, however, GFP-LC3 dots appeared after 24 h starvation in muscle tissues (Figure 7B). On the other hand, in brain samples, including the cerebral cortex and medulla oblongata, no GFP-LC3 structures could be detected in spite of 24 h starvation (Figures 7D and F). In addition, islets starved for 24 h stained faintly for insulin (middle panels, Figure 6). The mean insulin staining intensity of starved islets was markedly reduced compared with that of untreated control islets, although the difference in insulin intensity was

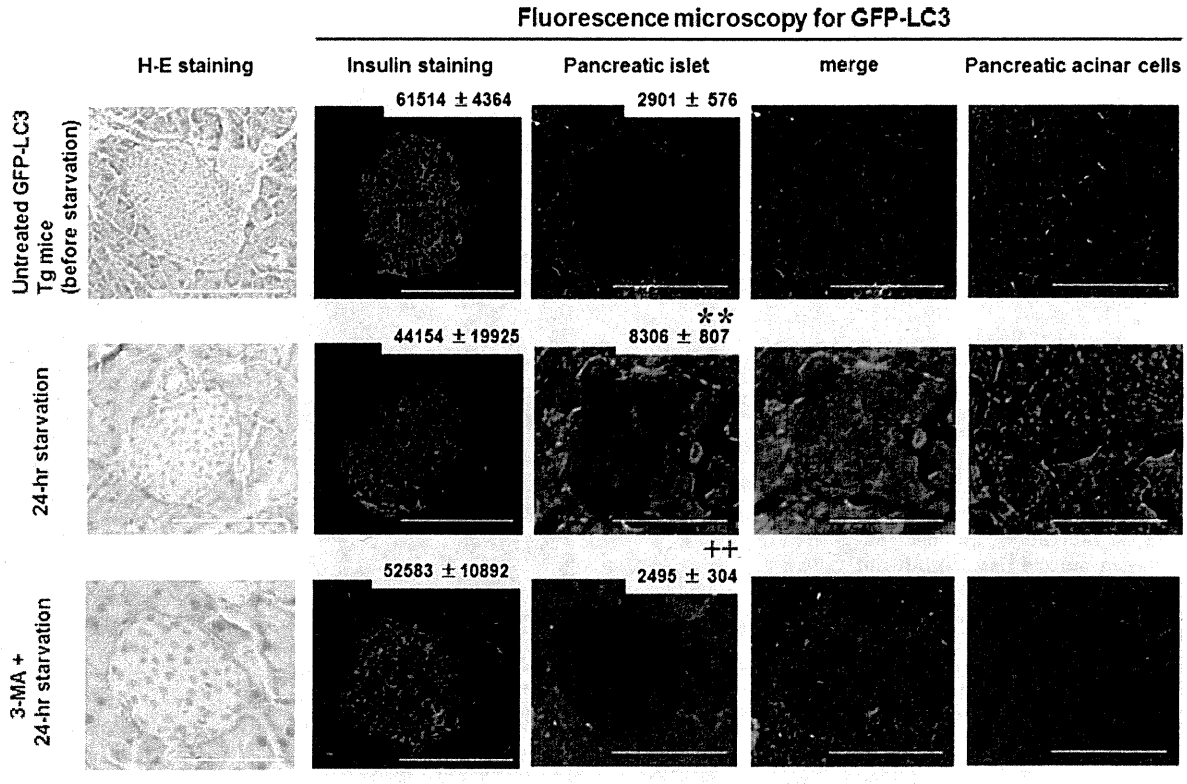

Figure 6: Starvation induced autophagy in pancreatic islets and acinar cells of GFP-LC3 transgenic mice. Representative images of islets stained with H&E and for insulin after 24 h starvation. Representative GFP images of pancreatic islets, acinar cells and merged microphotographs of GFP images and insulin staining. Numbers in the right upper corner of the photographs represent the mean ± SD intensity of GFP and insulin staining, expressed in arbitrary units, of five different islets. **$p < 0.01$, compared with the control; $^{++}p < 0.01$, compared with 24 h starvation. Bars = 100 μm.

not significant (control, 61 514 ± 4364; starvation, 44 154 ± 19 925). The mean fluorescence intensity of GFP-dots was significantly higher in starved islets than untreated control islets (control, 2901 ± 576; starvation, 8306 ± 807; $p < 0.01$). The merged images of GFP signals of LC3 dots and the adjacent islets stained for insulin are shown in Figure 6. The merged microphotographs also showed weaker insulin intensity in starved islets compared with the control islets. The use of 3-MA during 24 h starvation ameliorated the effect of 24 h starvation as evident by the appearance—diffuse and few fluorescence signals of GFP-LC3 dots—and by the return of GFP fluorescence intensity in islets. Furthermore, the recovered islets stained positive for insulin and the intensity of such staining was similar to the control islets, as judged by both the mean staining intensity and the merged microphotographs (lower panels, Figure 6).

Effect of rapamycin on autophagy in GFP-LC3 transgenic mice

Finally, we assessed the effects of rapamycin on autophagy and insulin production in transgenic mice *in vivo*. For this purpose, the mice were treated with 0.2 mg/kg of rapamycin intraperitoneally daily for 1, 2, 3, 4 or 5 weeks. After 1 week of such treatment, small but few dots appeared in both islets and acinar cells, however, no significant difference was observed in the pancreas of rapamycin-treated mice and rapamycin-plus-3-MA (10 mM)-treated mice (top panels, Figures 8A and B). After 2, 3, 4 and 5 weeks of rapamycin treatment, a marked increase in the density of GFP-LC3 dots was observed and these dots appeared as ring- or cup-shaped structures in both islets and acinar cells (Figures 8A and B). The GFP fluorescence intensity was higher in 1-week treated islets than in untreated control islets, although no significant large GFP dots were observed (Figures 6 and 8A). After 2, 3, 4 and 5 weeks of treatment, the GFP fluorescence intensity in the treated islets was significantly up-regulated compared with those in control and 1-week treated islets. In spite of overinduction of autophagy in rapamycin-treated islets, the mean intensities of insulin in 2-, 3-, 4- and 5-week rapamycin-treated islets were significantly lower than the control untreated islets (Figure 8A). Interestingly, 3-MA ameliorated the changes in immunofluorescence, including GFP-LC3 dots and insulin staining intensity, which reflects rapamycin-induced overinduction of autophagy (Figure 8B). The merged

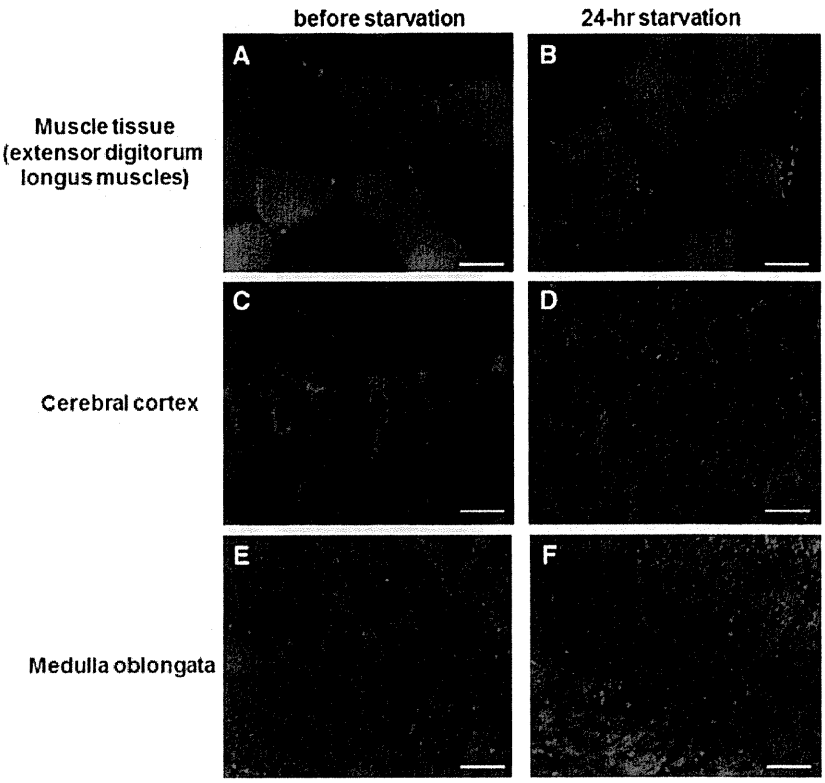

Figure 7: Starvation induced autophagy in muscle tissues, but not in brain. GFP images of transverse sections of extensor digitorum longus muscle (A) before starvation and (B) after starvation. GFP images of the cerebral cortex (C) before starvation and (D) after starvation. GFP images of medulla oblongata (E) before starvation and (F) after starvation. Bars = 10 μm.

microphotographs also demonstrated reduced insulin intensity in rapamycin-treated islets and that the degenerative change showed significant recovery in islets of the rapamycin-plus-3-MA group. TUNEL-positive cells were detected in 2-, 3-, 4- and 5-week rapamycin treated islets. In contrast, no such cells were observed in islets treated with rapamycin-plus-3-MA. Taken together, these *in vivo* findings correlated well with the *in vitro* data, including islet insulin potency and TMRE viability assay.

To further determine the effects of rapamycin on islet function in mice, we measured nonfasting blood glucose and plasma insulin concentrations. Rapamycin had no significant effect on nonfasting blood glucose levels, and near-normoglycemia was noted in mice treated with rapamycin alone and in those treated with rapamycin-plus-3-MA (Figures 9A and B). At days 14, 21, 28 and 35 after treatment, plasma insulin levels were higher in rapamycin-plus-3-MA-treated mice than in rapamycin-treated mice. Especially, plasma insulin concentration at day 14 in rapamycin-treated mice was significantly lower than in rapamycin-plus-3-MA-treated mice (Figures 9C and D). All other differences in insulin concentration were not significant between the two groups. Interestingly, in IPGTT performed at day 14, the blood glucose level of mice treated with rapamycin alone was significantly higher than in those treated with rapamycin-plus-3-MA at 15, 30, 60, 90 and 120 min after injection of glucose. Thus, rapamycin elicited a diabetic glucose pattern in mice (Figure 9E). In contrast, in the same test performed at day 28, the blood glucose levels of rapamycin-treated mice were similar to those of mice treated with rapamycin-plus-3-MA, and the pattern of blood glucose after injection was also similar between the two groups (Figure 9F). Taken together, rapamycin treatment resulted in impairment of *in vivo* glucose tolerance until 2 weeks after treatment and this abnormality was reversed by co-administration of 3-MA. It is possible that this abnormality of glucose tolerance represents physiological adjustment, such as reduction of insulin resistance at day 28. Further analysis of this phenomenon requires *in vivo* experiments of long-term rapamycin treatment.

Discussion

Rapamycin has deleterious effects on islet β cell based on the blockade of VEGF-mediated survival pathways and inhibition of β-cell proliferation and by induction of apoptosis (20,34,42). Accordingly, we raised the question of whether rapamycin in islet transplantation is a friend or a foe. In this study, we focused on the effect of rapamycin on autophagy and evaluated the direct effect of rapamycin on islet β cells. Using various techniques, the results demonstrated for the first time that rapamycin at therapeutically used concentrations, overinduced autophagy both *in vitro* and *in vivo* and that this effect on islet β cells impaired both islet viability and insulin potency.

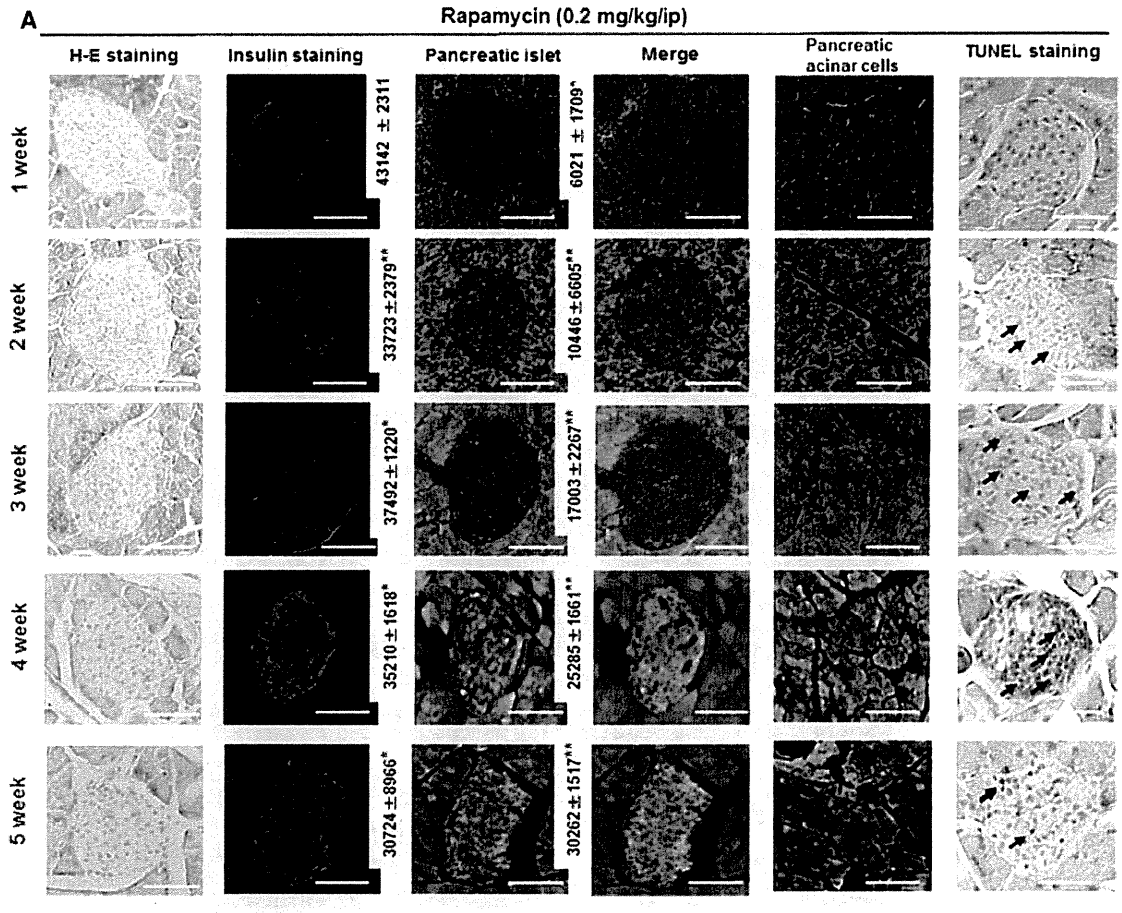

Figure 8: Upregulation of autophagy in rapamycin-treated GFP-LC3 transgenic mice. Representative images of islets stained with H&E, GFP images of pancreatic islets and acinar cells, images of islets stained for insulin and images of TUNEL staining after the indicated period of treatment. Also shown are the merged microphotographs of GFP images and insulin staining. Numbers in the right upper corner of the photographs represent the mean ± SD intensity of GFP and insulin staining, expressed in arbitrary units, of five different islets. *$p < 0.05$, compared with the control; **$p < 0.01$, compared with the control; $^{++}p < 0.01$, compared with rapamycin alone. Images were obtained from GFP-LC3 transgenic mice treated with (A) 0.2 mg/kg/i.p. rapamycin alone and (B) 0.2 mg/kg/i.p. rapamycin-plus-10 mM 3-MA. Bars = 100 μm.

Autophagy is the degradation of redundant or faulty cell components (1–4,12). Recent studies have described a link between diabetes and autophagy (43,44). Two groups independently reported the findings of increased apoptosis and reduced proliferation of β cells with resultant reduction in β-cell mass in β-cell-specific autophagy-deficient mice ($Atg7^{f/f}$: RIP-Cre mice; Refs. 43,44). These studies indicated that basal autophagy is indispensable for the maintenance of normal islet architecture, such as mitochondria and function of β cells (43,44).

As shown in Figure 1 and immunoblot analyses reported by others (36,44–46), endogenous LC3-II expression was detected in cell lysates from pancreatic islets and a low level of constitutive autophagy (here referred to as "basal autophagy") was present in normal control islets. Our results also showed that rapamycin resulted in overinduction of autophagy in islets with consequent impairment of insulin function, both *in vitro* and *in vivo*. These results suggest that overinduction of autophagy by rapamycin in islet β cells negatively affects insulin function by modulating cell death through accelerated self-digestion and degradation of essential cellular components. Based on the effect of rapamycin on islet β cells, it is possible that excessive digestion of various types of cellular structures, including insulin granules, mitochondria and endoplasmic reticulum membranes takes place in autophagic vacuoles, because this structure lacks stringent substrate specificity, which is different from that used by the ubiquitin–proteasome system (47); in other words, any structure in the cytosol could become a substrate for autophagy (43,44). This may explain the significantly low insulin production capacity of *in vitro*

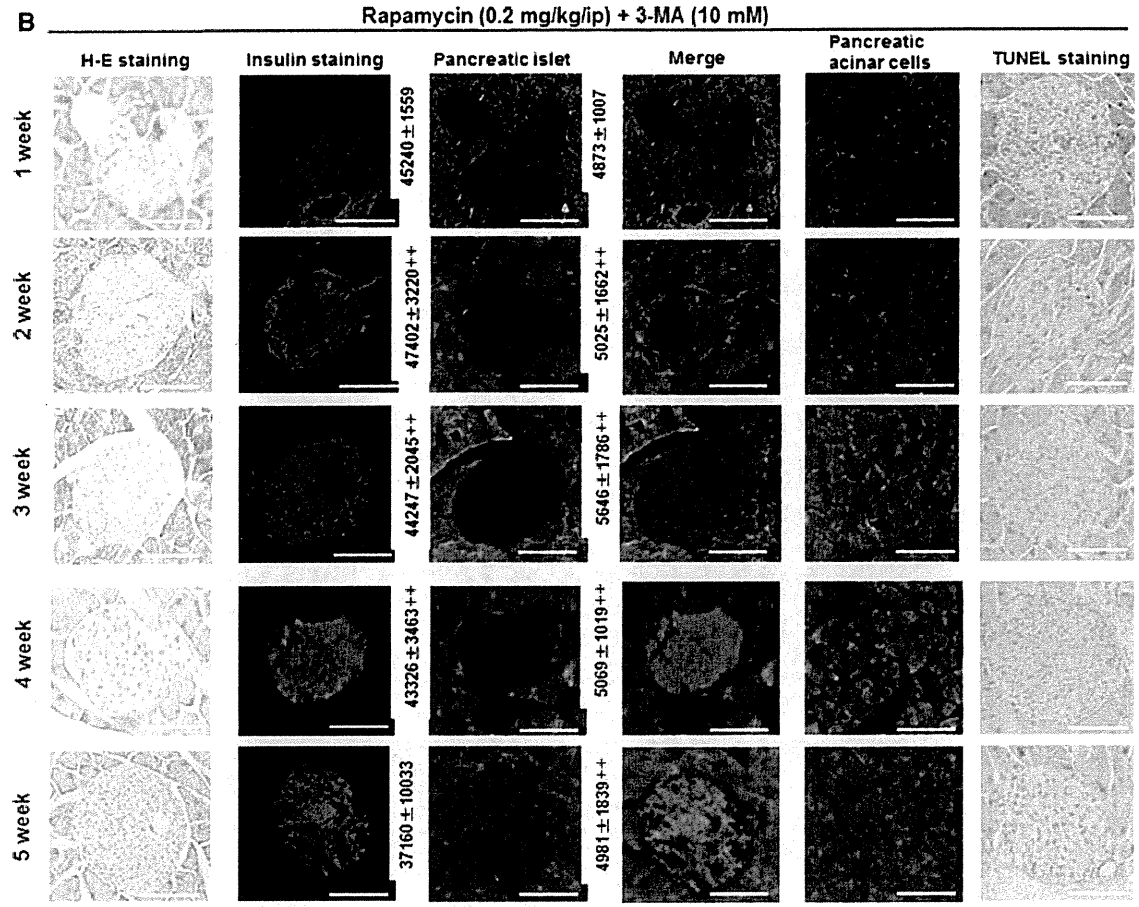

Figure 8: Continued.

rapamycin-treated islet β cells, the significant reduction of insulin staining intensity in islets of rapamycin-treated mice and the marked impairment of glucose tolerance assessed by IPGTT (Figures 5, 8A and 9E). Based on these results, we speculate that the main etiology of progressive dysfunction of transplanted islets is reduced insulin production related to rapamycin treatment and the related overinduction of autophagy.

Although the protective role of basal autophagy on pancreatic β-cell function has been proposed in loss-of-function studies on Atg/genes (43,44,48), accelerated autophagy seems to be involved in certain types of cell death (2,49–51). For this reason, we evaluated β-cell apoptosis by TMRE staining and TUNEL, and dead cells by 7-AAD. Figures 4A and B showed that rapamycin increased the percentages of apoptotic β cells and 7-AAD-positive dead islet cells. Furthermore, the TUNEL-positive apoptotic cells were observed in islets of rapamycin-treated mice and these apoptotic cells disappeared after the administration of 3-MA. These findings seem to indicate the existence of crosstalk between autophagy and apoptosis and various links between autophagy and cell death, which may occur in a hierarchial or independent fashion (52–55). In this regard, Masini et al. (48) reported that exposure of nondiabetic islets to high concentrations of free fatty acid resulted in accumulation of autophagic vacuoles. Together with enhanced β-cell death, which was associated with decreased LAMP2 expression. These results suggest that accelerated autophagy may contribute to β-cell death under special conditions, such as rapamycin treatment.

The upregulation of autophagy after rapamycin treatment resulted in a significant impairment of β-cell insulin function, and this effect may contribute to islet graft dysfunction observed in islet recipients. We also demonstrated that 3-MA ameliorated rapamycin-related β-cell dysfunction both *in vitro* and *in vivo*. Thus, this new modulator of autophagy, such as 3-MA, should be tested further clinically, and better therapeutic agents with specific autophagic activity need to be developed for the prevention and treatment of islet graft dysfunction.

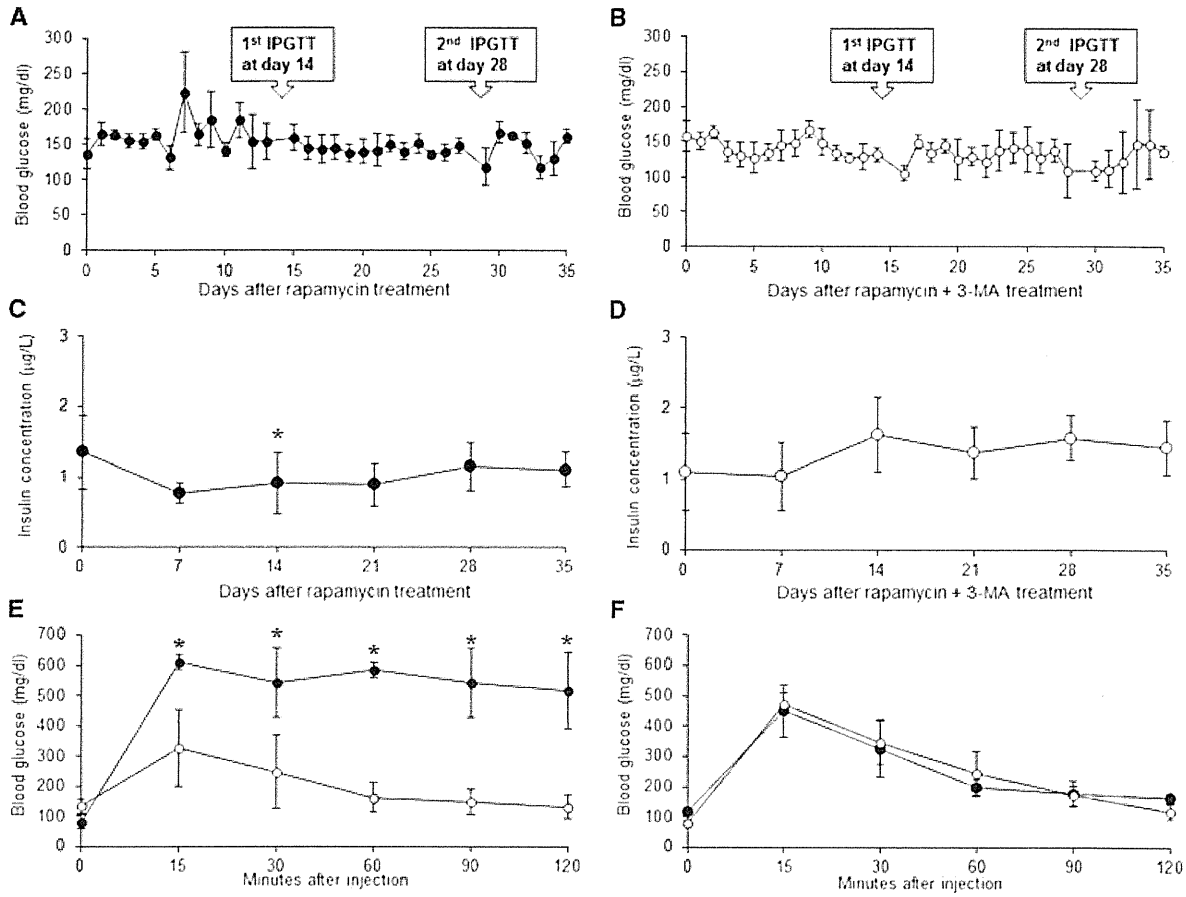

Figure 9: Nonfasting blood glucose and plasma insulin concentrations after treatment and glucose tolerance test at days 14 and 28. (A) Blood glucose level of GFP-LC3 transgenic mice treated with 0.2 mg/kg/i.p. rapamycin alone. (B) Blood glucose level of GFP-LC3 transgenic mice treated with 0.2 mg/kg/i.p. rapamycin-plus-10 mM 3-MA. (C) Plasma insulin concentration of mice treated with 0.2 mg/kg/i.p. rapamycin alone. (D) Plasma insulin concentration of mice treated with 0.2 mg/kg/i.p. rapamycin-plus-10 mM 3-MA. (E) Glucose tolerance test after treatment at day 14. (F) Glucose tolerance test after treatment at day 28. Closed circles: data of mice treated with 0.2 mg/kg/i.p. rapamycin alone; open circles: data of mice treated with 0.2 mg/kg/i.p. rapamycin-plus-10 mM 3-MA. Data are mean ± SD of five mice in each treatment group.

Acknowledgments

The authors thank Dr. F.G. Issa (www.word-medex.com.au) for the careful reading and editing of the manuscript. We also thank Dr. N. Kawaguchi and Prof. N. Matsuura (Osaka University) for their help in the execution of this project and the valuable suggestions.

Funding source: This work was supported by a grant from the Ministry of Education, Sports and Culture of Japan to M. T. (No. 22591520) and by Kobayashi Foundation for Cancer Research to M. T.

Disclosure

The authors of this manuscript have no conflicts of interest to disclose as described by the *American Journal of Transplantation.*

References

1. Levine B, Klionsky DJ. Development by self-digestion: Molecular mechanisms and biological functions of autophagy. Dev Cell 2004; 6: 463–477.
2. Levine B, Kroemer G. Autophagy in the pathogenesis of disease. Cell 2008; 132: 27–42.
3. Mizushima N, Yoshimori T, Levine B. Methods in mammalian autophagy research. Cell 2010; 140: 313–326.
4. Kuma A, Hatano M, Matsui M, et al. The role of autophagy during the early neonatal starvation period. Nature 2004; 432: 1032–1036.
5. Ravikumar B, Vacher C, Berger Z, et al. Inhibition of mTOR induces autophagy and reduces toxicity of polyglutamine expansions in fly and mouse models of Huntington disease. Nat Genet 2004; 36: 585–595.
6. Hara T, Nakamura K, Matsui M, et al. Suppression of basal autophagy in neural cells causes neurodegenerative disease in mice. Nature 2006; 441: 885–889.

7. Komatsu M, Waguri S, Chiba T, et al. Loss of autophagy in the central nervous system causes neurodegeneration in mice. Nature 2006; 441: 880–884.
8. Levine B. Cell biology: Autophagy and cancer. Nature 2007; 446: 745–747.
9. Nakai A, Yamaguchi O, Takeda T, et al. The role of autophagy in cardiomyocytes in the basal state and in response to hemodynamic stress. Nat Med 2007; 13: 619–624.
10. Virgin HW, Levine B. Autophagy genes in immunity. Nat Immunol 2009; 10: 461–470.
11. Levine B, Mizushima N, Virgin HW. Autophagy in immunity and inflammation. Nature 2011; 469:323–335.
12. Mizushima N. The pleiotropic role of autophagy: From protein metabolism to bactericide. Cell Death Differ 2005; 12: 1535–1541.
13. Abraham RT. Mammalian target of rapamycin: Immunosuppressive drugs uncover a novel pathway of cytokine receptor signaling. Curr Opin Immunol 1998; 10: 330–336.
14. Augustine JJ, Bodziak KA, Hricik DE. Use of sirolimus in solid organ transplantation. Drugs 2007; 67: 369–391.
15. Kirken RA, Wang YL. Molecular actions of sirolimus: Sirolimus and mTor. Transplant Proc 2003; 35 (Suppl 3): 227S-230S.
16. Hay N, Sonenberg N. Upstream and downstream of mTOR. Genes Dev 2004; 18: 1926–1945.
17. Schmelzle T, Hall MN. TOR, a central controller of cell growth. Cell 2000; 103: 253–262.
18. Shapiro AM, Lakey JR, Ryan EA, et al. Islet transplantation in seven patients with type 1 diabetes mellitus using a glucocorticoid-free immunosuppressive regimen. N Engl J Med 2000; 343: 230–238.
19. Ryan EA, Lakey JR, Rajotte RV, et al. Clinical outcomes and insulin secretion after islet transplantation with the Edmonton protocol. Diabetes 2001; 50: 710–719.
20. Markmann JF, Deng S, Huang X, et al. Insulin independence following isolated islet transplantation and single islet infusions. Ann Surg 2003; 237: 741–749.
21. Froud T, Ricordi C, Baidal DA, et al. Islet transplantation in type 1 diabetes mellitus using cultured islets and steroid-free immunosuppression: Miami experience. Am J Transplant 2005; 5: 2037–2046.
22. Hering BJ, Wijkstrom M. Sirolimus and islet transplants. Transplant Proc 2003; 35 (Suppl 3): 187S–190S.
23. Li Y, Li XC, Zheng XX, et al. Blocking both signal 1 and signal 2 of T-cell activation prevents apoptosis of alloreactive T cells and induction of peripheral allograft tolerance. Nat Med 1999; 5: 1298–1302.
24. Battaglia M, Stabilini A, Draghici E, et al. Induction of tolerance in type 1 diabetes via both CD4+CD25+ T regulatory cells and T regulatory type 1 cells. Diabetes 2006; 55: 1571–1580.
25. Ryan EA, Paty BW, Senior PA, et al. Five-year follow-up after clinical islet transplantation. Diabetes 2005; 54: 2060–2069.
26. Desai NM, Goss JA, Deng S, et al. Elevated portal vein drug levels of sirolimus and tacrolimus in islet transplant recipients: Local immunosuppression or islet toxicity? Transplantation 2003; 76: 1623–1625.
27. Ricordi C, Zeng YJ, Alejandro R, et al. *In vivo* effect of FK506 on human pancreatic islets. Transplantation 1991; 52: 519–522.
28. Heit JJ, Apelqvist AA, Gu X, et al. Calcineurin/NFAT signalling regulates pancreatic beta-cell growth and function. Nature 2006; 443: 345–349.
29. Zhang N, Su D, Qu S, et al. Sirolimus is associated with reduced islet engraftment and impaired beta-cell function. Diabetes 2006; 55: 2429–2436.
30. Bell E, Cao X, Moibi JA, et al. Rapamycin has a deleterious effect on MIN-6 cells and rat and human islets. Diabetes 2003; 52: 2731–2739.
31. Lopez-Talavera JC, Garcia-Ocaña A, Sipula I, et al. Hepatocyte growth factor gene therapy for pancreatic islets in diabetes: Reducing the minimal islet transplant mass required in a glucocorticoid-free rat model of allogeneic portal vein islet transplantation. Endocrinology 2004; 145: 467–474.
32. Cantaluppi V, Biancone L, Romanazzi GM, et al. Antiangiogenic and immunomodulatory effects of rapamycin on islet endothelium: Relevance for islet transplantation. Am J Transplant 2006; 6: 2601–2611.
33. Miriuka SG, Rao V, Peterson M, et al. mTOR inhibition induces endothelial progenitor cell death. Am J Transplant 2006; 6: 2069–2079.
34. Zahr E, Molano RD, Pileggi A, et al. Rapamycin impairs *in vivo* proliferation of islet beta-cells. Transplantation 2007; 84: 1576–1583.
35. Li X, Zhang L, Meshinchi S, et al. Islet microvasculature in islet hyperplasia and failure in a model of type 2 diabetes. Diabetes 2006; 55: 2965–2973.
36. Mizushima N, Yamamoto A, Matsui M, et al. *In vivo* analysis of autophagy in response to nutrient starvation using transgenic mice expressing a fluorescent autophagosome marker. Mol Biol Cell 2004; 15: 1101–1111.
37. Johnson AL, Ratajczak C, Haugen MJ, et al. Tumor necrosis factor-related apoptosis inducing ligand expression and activity in hen granulosa cells. Reproduction 2007; 133: 609–616.
38. Ichii H, Pileggi A, Molano RD, et al. Rescue purification maximizes the use of human islet preparations for transplantation. Am J Transplant 2005; 5: 21–30.
39. Ichii H, Wang X, Messinger S, et al. Improved human islet isolation using nicotinamide. Am J Transplant 2006; 6: 2060–2068.
40. Sawada T, Matsumoto I, Nakano M, et al. Improved islet yield and function with ductal injection of University of Wisconsin solution before pancreas preservation. Transplantation 2003; 75: 1965–1969.
41. Andrikopoulos S, Blair AR, Deluca N, Fam BC, Proietto J. Evaluating the glucose tolerance test in mice. Am J Physiol Endocrinol Metab 2008; 295: E1323–E1332.
42. Laugharne M, Cross S, Richards S, et al. Sirolimus toxicity and vascular endothelial growth factor release from islet and renal cell lines. Transplantation 2007; 83: 1635–1638.
43. Jung HS, Chung KW, Won Kim J, et al. Loss of autophagy diminishes pancreatic beta cell mass and function with resultant hyperglycemia. Cell Metab 2008; 8: 318–324.
44. Ebato C, Uchida T, Arakawa M, et al. Autophagy is important in islet homeostasis and compensatory increase of beta cell mass in response to high-fat diet. Cell Metab 2008; 8: 325–332.
45. Mariño G, Salvador-Montoliu N, Fueyo A, et al. Tissue-specific autophagy alterations and increased tumorigenesis in mice deficient in Atg4C/autophagin-3. J Biol Chem 2007; 282: 18573–18583.
46. Fujitani Y, Kawamori R, Watada H. The role of autophagy in pancreatic beta-cell and diabetes. Autophagy 2009; 5: 280–282.
47. Coux O, Tanaka K, Goldberg AL. Structure and functions of the 20S and 26S proteasomes. Annu Rev Biochem 1996; 65: 801–847.
48. Masini M, Bugliani M, Lupi R, et al. Autophagy in human type 2 diabetes pancreatic beta cells. Diabetologia 2009; 52: 1083–1086.
49. Shintani T, Klionsky DJ. Autophagy in health and disease: A double-edged sword. Science 2004; 306: 990–995.
50. Fujitani Y, Ueno T, Watada H. Autophagy in health and disease. 4. The role of pancreatic beta-cell autophagy in health and diabetes. Am J Physiol Cell Physiol 2010; 299: C1–C6.
51. Marsh BJ, Soden C, Alarcón C, et al. Regulated autophagy controls hormone content in secretory-deficient pancreatic endocrine beta-cells. Mol Endocrinol 2007; 21: 2255–2269.

52. Moretti L, Cha YI, Niermann KJ, Lu B. Switch between apoptosis and autophagy: Radiation-induced endoplasmic reticulum stress? Cell Cycle 2007; 6: 793–798.
53. Maiuri MC, Zalckvar E, Kimchi A, Kroemer G. Self-eating and self-killing: Crosstalk between autophagy and apoptosis. Nat Rev Mol Cell Biol 2007; 8: 741–752.
54. Marchetti P, Masini M. Autophagy and the pancreatic beta-cell in human type 2 diabetes. Autophagy 2009; 5: 1055–1066.
55. Liu JJ, Lin M, Yu JY, Liu B, Bao JK. Targeting apoptotic and autophagic pathways for cancer therapeutics. Cancer Lett 2011; 300: 105–114.

Supporting Information

Additional Supporting Information may be found in the online version of this article.

Supplementary Materials and Methods

Please note: Wiley-Blackwell is not responsible for the content or functionality of any supporting materials supplied by the authors. Any queries (other than missing material) should be directed to the corresponding author for the article.

Hypoxia and *TP53* deficiency for induced pluripotent stem cell-like properties in gastrointestinal cancer

HIROMITSU HOSHINO[1], HIROAKI NAGANO[1], NAOTSUGU HARAGUCHI[2], SHIMPEI NISHIKAWA[1], AKIRA TOMOKUNI[1], YOSHIHIRO KANO[1], TAKAHITO FUKUSUMI[1], TOSHIYUKI SAITO[3], MIYUKI OZAKI[2], DAISUKE SAKAI[2], TAROH SATOH[2], HIDETOSHI EGUCHI[1], MITSUGU SEKIMOTO[1], YUICHIRO DOKI[1,2], MASAKI MORI[1,2*] and HIDESHI ISHII[1-3*]

Departments of [1]Gastroenterological Surgery, [2]Frontier Science for Cancer and Chemotherapy, Osaka University Graduate School of Medicine, Suita, Osaka 565-0871; [3]Transcriptome Profiling Group, National Institute of Radiological Sciences, Research Center for Charged Particle Therapy, Chiba 263-8555, Japan

Received October 14, 2011; Accepted December 1, 2011

DOI: 10.3892/ijo.2012.1346

Abstract. Induced pluripotent stem (iPS)-like cancer cells (iPC) by the introduction of defined transcription factors reduce the prevalence of the malignant phenotype of digestive system cancer cells, but the induction efficiency is low. The role of hypoxia and *TP53* deficiency in iPC cell generation remain unclear. Cellular reprogramming was performed by retroviral infection with *OCT3/4, SOX2, KLF4* and *c-MYC* of wild-type HCT116 colorectal cancer cells and mutant *TP53*-deficient HCT116 cells. Cells were cultured in normoxia (21% O_2) or hypoxia (5% O_2) for 30 days after transduction, and the response to hypoxia and comparison of cellular proliferation, invasion and tumourigenesis before and after iPC cell generation were studied. iPC cell generation from wild-type HCT116 cells in hypoxia was approximately 4-times greater than in normoxia ($p<0.05$), and *TP53* deficiency increased conversion efficiency significantly in normoxia ($p<0.05$). Significant involvement of hypoxia-inducible factors was observed in an immature carbohydrate epitope, Tra-1-60$^+$, colony formation. Generated iPC cells exhibited multi-differentiation potential. Although the iPC cells in hypoxia exhibited reduced proliferation, invasiveness and tumourigenicity, *TP53* deficiency in iPC cells resulted in higher tumourigenicity than in wild-type cells. Both hypoxia and *TP53* deficiency increase iPC cell generation. *TP53* deficiency can also result in deleterious mutations, whereas hypoxia may impact molecular targets of epigenome normalisation.

Correspondence to: Professor Masaki Mori, Department of Gastroenterological Surgery, Osaka University Graduate School of Medicine, Yamadaoka 2-2, Suita, Osaka 565-0871, Japan
E-mail: mmori@gesurg.med.osaka-u.ac.jp

Professor Hideshi Ishii, Department of Frontier Science for Cancer and Chemotherapy, Osaka University Graduate School of Medicine, Yamadaoka 2-2 (E21-19), Suita, Osaka 565-0871, Japan
E-mail: hishii@gesurg.med.osaka-u.ac.jp

*Contributed equally

Key words: cancer reprogramming, epigenome normalisation, hypoxia, tumour suppressor genes

Introduction

Although disruption of the normal differentiation process is an important component of tumourigenesis (1) and is involved in leukaemogenesis (2) and the formation of other malignancies (3), not much is understood about the reversibility of this process. In general, genetic alterations such as mutations (substitutions of nucleotide sequences), amplifications and deletions, as well as recurring chromosomal aberrations are irreversible, whereas epigenetic alterations can be modified by pharmacological agents that target components of the epigenetic machinery (4). Since epigenetic modifications, including DNA methylation and histone modifications, substantially contribute to the tumour cell phenotype, the number of potential therapeutic targets has increased (5). Epigenome normalisation is a potential therapeutic approach for cancer treatment in the clinical setting and in translational aspects of epigenetic research (5).

An important discovery that has been reported is that complete reprogramming can be achieved by the introduction of defined transcription factors, Oct4 (also known as Pou5f1), Sox2, Klf4 and cMyc, from terminally differentiated somatic fibroblasts (6). Generation of induced pluripotent stem (iPS) cells is believed to require epigenetic modifications, but the precise mechanism is unknown (7). Recently, we showed that introducing defined factors in gastrointestinal cancer cells resulted in the acquisition of multi-differentiation potential, i.e. the gene expression profiles of mesoderm and ectoderm appeared in gastrointestinal cancer cells of endodermal origin [iPS-like cancer (iPC) cells] (8). Reprogramming of sensitised cancer cells in response to differentiation therapy suppressed tumourigenicity *in vivo* (8); this presumably involved reactivation of tumour suppressor genes at the *CDKN2b-CDKN2a* locus on chromosome 9p21 in humans (chromosome 4 in mice), a region that is frequently inactivated in cancer and

is involved in the reduction of chemosensitivity (9). Together, these findings strongly suggest that the magnitude of epigenetic modifications using iPS technology may be sufficient to reverse the differentiation programme and lead to a multipotent state as well as contribute to the suppression of biologically malignant phenotypes in cancer cells.

Recent studies have shown that silencing or absence of p53 significantly increases iPS cell generation (10-12). Another study demonstrated that hypoxia enhance iPS cell generation in humans and mice (13). Since p53 activation characterises cancer cells that survive in hypoxia (14,15), it is possible that reprogramming of cancer cells may be closely associated with the p53 and hypoxic pathways. Herein, we studied these pathways and demonstrated that although prolonged *in vitro* culture increased tumourigenic potential in *TP53*-deficient iPC cells, hypoxia and *TP53* deficiency enhances iPC cell generation. This suggests that *TP53* deficiency functions as a two-edged sword and that *TP53* is a candidate molecular marker for predicting the biological behaviour of reprogrammed cancer cells.

Materials and methods

Cell lines and culture. Wild-type (wt) and TP53-deficient colorectal cancer (CRC) cell lines, wt HCT116 cells and its homologous-recombination mutant, HCT116 p53-deficient (null) cells, were donated by Dr Bert Vogelstein (Johns Hopkins University, Baltimore, MD, USA), and other cancer cell lines were obtained from DS Pharma Biomedical Co., Ltd. (Osaka, Japan). Cell lines were maintained in Dulbecco's modified Eagle's medium (DMEM; Nacalai Tesque, Kyoto, Japan) supplemented with 10% foetal bovine serum (FBS) at 37˚C in a 5% humidified CO_2 atmosphere. Plasmids were purchased from Addgene (Cambridge, MA). Transfectants were grown in DMEM supplemented with 10% FBS and puromycin (2 μg/ml) and subsequently incubated in specific culture conditions as described previously (8). All retroviral transfections were performed using ViraDuctin Transduction kit (Cell Biolabs, San Diego, CA). Transfections with lentivirus were performed using the Virapower Lentiviral Packaging mix (Invitrogen, Carlsbad, CA). In brief, cancer cell lines were transfected with plasmids at a concentration of 4 μg/μl using Lipofectamine 2000 (Invitrogen) and incubated in glucose-free Opti-MEM (Invitrogen). These transfected cell lines were cultured in 21% or 5% CO_2. All experiments were performed at 50-70% cell confluence and results were confirmed in at least three independent experiments. All-in-one type fluorescence microscope (BZ-8000; Keyence, Osaka, Japan) with digital photographic capability was used to visualise cells at several magnifications. In the proliferation assay, growth rates of the cultured gastrointestinal cancer cell lines were measured by counting cells using Celltac (Nihon Kohden Co., Tokyo, Japan).

RNA preparation and real-time reverse transcription-polymerase chain reaction (qRT-PCR). Total RNA was prepared using TRIzol reagent (Invitrogen). RT was performed using SuperScript III RT kits (Invitrogen). To confirm PCR amplification, 25-35 cycles of PCR were performed using a PCR kit (Takara, Kyoto, Japan) on the GeneAmp PCR System 9600 (PE Applied Biosystems, Foster City, CA) in the following conditions: 95˚C for 10 sec, 60˚C for 10 sec and 72˚C for 60 sec. An 8-μl aliquot of each reaction mixture was size-fractionated in a 1.5% agarose gel and visualised by ethidium bromide staining. To confirm RNA quality, PCR amplification was performed for *GAPDH* using specific primers. For quantitative assessment, the gene expression was evaluated by qRT-PCR using a LightCycler TaqMan Master kit (Roche Diagnostics, Tokyo, Japan) for cDNA amplification of specific target genes. The expression of mRNA copies was normalised against *GAPDH* mRNA expression.

Reagents and antibodies. Antibodies against Nanog, Ssea-4, Tra-1-60, Tra-1-81 and Tra-2-49 (Chemicon International Inc., Temecula, CA) were used for immunocytology.

Invasion assay. Cell invasion was analysed using the CytoSelect assay kit according to the manufacturer's protocol (Cell Biolabs). Cells ($1.0x10^5$) in DMEM were placed on 8.0-μm pore-size membrane inserts in 96-well plates, and DMEM with 10% FBS was added to each well. After 24-h incubation at 37˚C in 5% CO_2, non-invading cells were removed from the top of the membrane chamber and cells on the underside of the membrane were completely dislodged by tilting the membrane chamber in cell detachment solution (Cell Biolabs). Lysis buffer/CyQuant GR dye solution (Cell Biolabs) was then added to each well, and fluorescence was determined at 480 or 520 nm using a plate reader to estimate the number of cells that had invaded the undersurface of the membrane. Each assay was performed in triplicate.

Tumourigenicity. Cells were subcutaneously inoculated into NOD/SCID mice. The tumour diameter and size were estimated using the following formula: size = $(\text{length})^2$ x (width)/2

Statistical analysis. For continuous variables, results are expressed as means ± standard errors. The relationship between the gene expression level and cell count was analysed by Chi-square and Wilcoxon rank tests. All data were analysed using JMP software (SAS Institute, Cary, NC). Differences with $p<0.05$ were considered statistically significant.

Results

Lentiviral- and retroviral-mediated iPS factor gene transfer. The expression profile of ES-like genes is reportedly associated with aggressive phenotypes observed in solid tumours (16). Considering that reprogramming induces the endogenous expression of ES-like genes, it is assumed that the expression of endogenous genes may be involved in reprogramming and some cancer cells with a relatively higher expression of endogenous ES-like genes may be sensitive to reprogramming induction. We quantitatively studied the expression of endogenous immature *NANOG* by qRT-PCR (data not shown), because *NANOG* is not included in exogenously mediated reprogramming vectors in the present experiment but is relevant to the immature status of iPS cells (6,17). The *NANOG* expression level in HCT116 p53 null cells was equal to that in PANC-1 cells, but compared with that in NTERA teratoma cells it was ~20% greater, while the expression in wt HCT116 cancer cell lines was relatively low (data not shown). We thus selected two cells each from wt HCT116 cells, its derivative

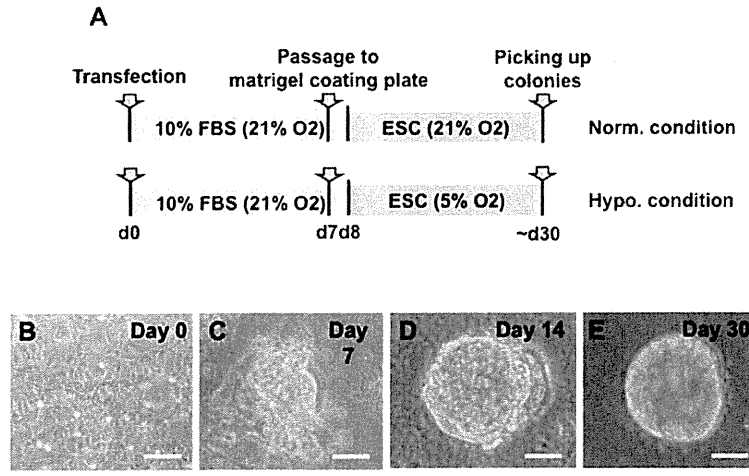

Figure 1. Retroviral- and lentiviral-mediated gene transfer of four iPS factor genes in gastrointestinal cancer cells. (A) Schematic representation of the experiment showing normoxia and hypoxia. (B-E) Morphological changes in iPC cells derived from pancreatic cancer wt HCT116 cells. (B) Day 0, (C) day 7, (D) day 14, (E) day 30 after transfection. Scale bar, 100 μm.

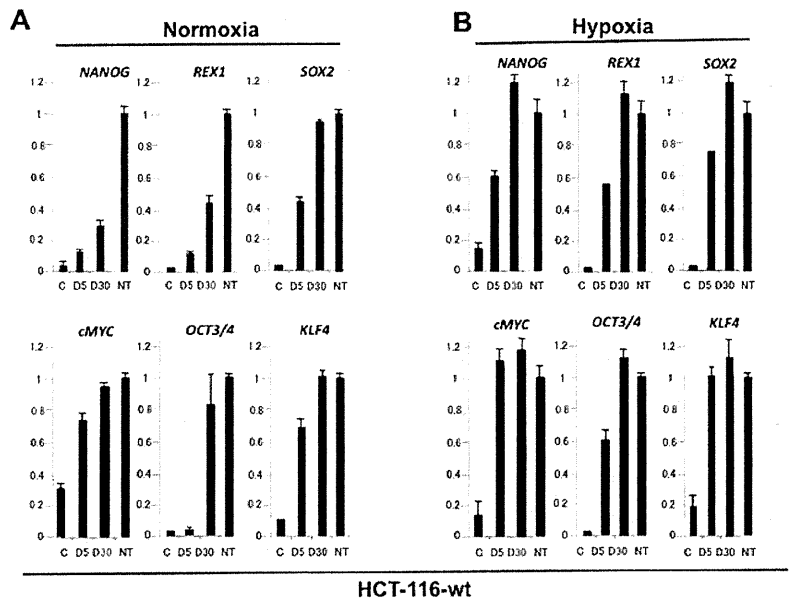

Figure 2. Exogenous and endogenous gene expression by iPS cells after retroviral- and lentiviral-mediated gene transfer in wt HCT116 cells. After viral vector-mediated gene transfer of the four defined factor genes *c-MYC, SOX2, OCT3/4* and *KLF4*, the expression of all exogenous and endogenous genes was assessed in normoxia (A) or hypoxia (B) on days 5 and 30 by qRT-PCR using specific primers.

line HCT116 p53 null cells and PANC-1 cells for comparison in subsequent experiments.

For the transfer of iPS factor genes, we infected cells on day 0 through lentiviral-mediated transfer of murine retroviral receptors followed by retroviral-mediated gene transfer of the four defined factor genes *c-MYC, SOX2, OCT3/4* and *KLF4*. On day 7, cells were transferred to ES culture medium in either hypoxia (5% O_2) or continuous normoxia (21% O_2) (Fig. 1A). The number of cells increased on day 7 and clear round colonies were formed by day 30 (representative data are shown in Fig. 1B-E). These induced cells were morphologically similar or indistinguishable from iPC cells derived from other gastrointestinal cancer cells (8) and were similar to iPS cells derived from terminally differentiated normal cells (7).

The expression in wt HCT116 and HCT116 p53 null cells of four exogenously introduced transgenes and endogenous genes in normoxia and hypoxia were analysed by qRT-PCR (Fig. 2, and data not shown). On day 5, the expression levels of exogenously introduced c-MYC, SOX2, OCT3/4 and KLF4 in wt HCT116 cells were 40%-80% and >60% and those of REX1 and NANOG, which were not introduced as transgenes, were ~10 and 60% of those in teratoma NTERA cells in normoxia and hypoxia, respectively (Fig. 2). These results suggested that compared with normoxia, hypoxia stimulates endogenous expression of ES-like genes, such as *REX1* and *NANOG*, and the relevance of this result was appreciable in assessment of four exogenously introduced transgenes and endogenous genes.

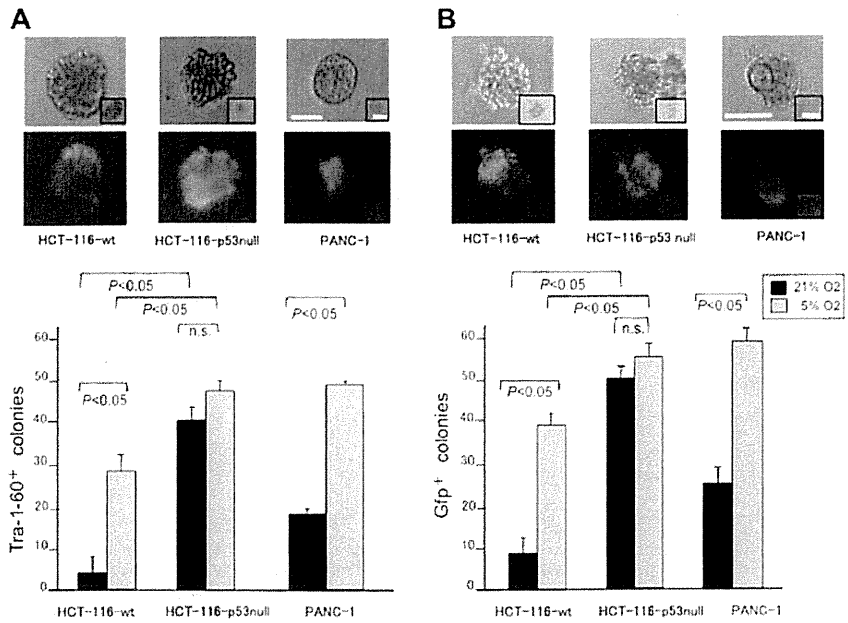

Figure 3. Effect of hypoxia on *TP53*-deficient cancer cells. The effects of reprogramming of wt HCT116, HCT116 p53 null and PANC-1 cells are shown by (A) immunostaining with anti-Tra-1-60 antibody or (B) observation of GFP-positive spheres under a fluorescence microscope on day 30. Reprogramming efficiency (percentage of Tra-1-60- or GFP-positive cells) in hypoxia (5% O_2) was higher than in normoxia (21% O_2). p-values are shown for each comparison. Scale bar, 50 μm.

On day 30, the expression levels of exogenously introduced *REX1* and *NANOG* were 30-40% and >100% and those of the endogenously introduced *c-MYC, SOX2* and *OCT3/4* were >80% of those in teratoma NTERA cells in normoxia and hypoxia, respectively (Fig. 2). By utilising specific primers, the assessment of exogenous expression levels on day 30 indicated that all transgenes in wt HCT116 cells had decreased to undetectable levels in normoxia and hypoxia, except for the expression levels of *c-MYC* in normoxia and hypoxia and *KLF4* in hypoxia, all of which persisted (data not shown). By day 30, the expression levels of all transgenes in HCT116 p53 null cells had decreased to undetectable levels in normoxia and hypoxia, except for the expression levels of *c-MYC* and *KLF4* in normoxia and hypoxia that persisted, and the expression levels were higher in hypoxia (data not shown). The overall trend of decreased exogenous gene expression levels is probably due to silencing of the introduced genes (7). Our data indicate that reprogramming factors elicited the specific activation of immature endogenous ES-like genes.

High expression of ES-like genes in hypoxia and TP53-deficient condition in iPC cells derived from gastrointestinal cancer. After the introduction of iPS factors, compared to the expression levels in wt HCT116 cells in normoxia and hypoxia, the expression levels of an immature carbohydrate epitope, Tra-1-60, in iPC cells derived from HCT116 p53 null cells was 8-times and 1.6-times greater ($p<0.05$, Fig. 3A), while those in PANC-1 cells was 2.4-times greater in hypoxia (5% O_2) than in normoxia (21% O_2) ($p<0.05$, Fig. 3A). These data indicate that p53-defiency induces reprogramming in normoxia, and to a lesser extent, in hypoxia, suggesting that the factors downstream of p53 signalling may be involved in increased reprogramming efficiency in hypoxia. On day 30, the increased expression of other immature carbohydrate epitopes and proteins, namely Tra-2-49, Tra-1-60, Tra-1-81, Ssea4 and Nanog, was confirmed by immunocytochemistry after the introduction of defined factors (data not shown).

For semi-quantitative analyses of *NANOG* promoter activity, the *NANOG* promoter fusion green fluorescent protein vector was co-transfected in iPC cell generation. The tracing study of *NANOG* promoter activity in iPC cells derived from HCT116 p53 null cells indicated that, compared with wt HCT116 cells, the endogenous *NANOG* promoter was activated after reprogramming in normoxia (5-times, $p<0.05$, Fig. 3B), and to a lesser extent in hypoxia (1.3-times, $p<0.05$, Fig. 3B). Similarly, *NANOG* promoter was activated in hypoxia in PANC-1 iPC cells (2.2-times, $p<0.05$, Fig. 3B). The data are consistent with the notion that reprogramming efficiency is increased by p53 deficiency and hypoxia in a common pathway. Although the observed *NANOG* reporter activity may reflect endogenous activity at a basal level (data not shown), the expression of Tra-1-60 seems to be more specific to reprogramming induction (6,17). We thus used Tra-1-60 to assess reprogramming in the following studies.

Previous studies indicated that the hypoxia-inducible factor (Hif) pathway plays a role in metabolic regulation of cancer, as in the p53 pathway (15). Thus, to determine whether Hif affects the downstream cellular response to reprogramming induction, we co-transfected cells with hydroxylation-defective active mutants *HIF1A-P402A/P564A* and *HIF2A-P405A/P531A*, which lack proline residues within the oxygen-dependent degradation domain. These residues are necessary for the interaction with von Hippel-Lindau tumour suppressor protein (pVHL) and their substitutions increase the stability of Hifs, because they resist proteasome-dependent degradation (15). qRT-PCR indicated that transgenes were detected for at least 5 days after transfection, which is the critical timeframe for reprogramming events involved in iPS generation (6,17). The Tra-1-60 expression data indicated that the introduction of

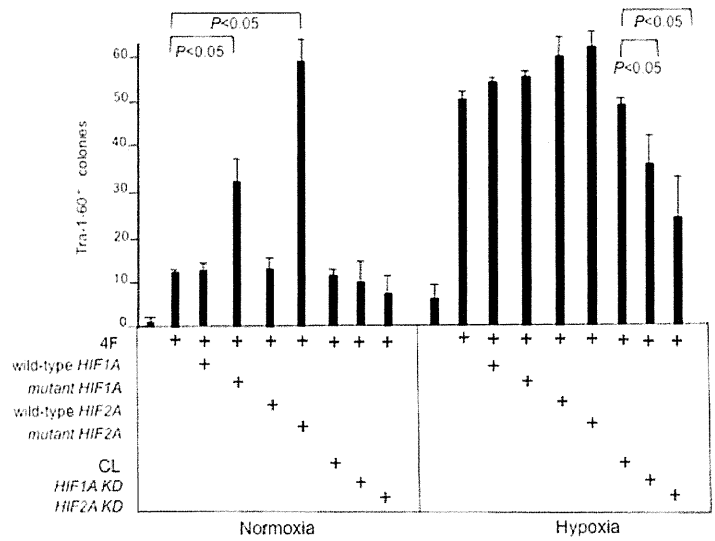

Figure 4. Efficiency of reprogramming induced by co-transfection with iPS factors and mutant *HIF* in wt HCT116 cells. Number of Tra-1-60$^+$ and GFP$^+$ clones as percentage of colonies on day 30 after gene transfer are shown. 4F, four factor genes *(c-MYC, SOX2, OCT3/4* and *KLF4)*; mutant *HIF1A*, the hydroxylation-defective mutant *HIF1A-P402A/P564A* lacking proline residues that are necessary for the interaction with pVHL and are refractory to proteasome-dependent degradation; mutant *HIF2A*, the hydroxylation-defective mutant *HIF2A-P405A/P531A*; *HIF1A KD*, lentiviral shRNA knockdown of *HIF1A*; *HIF2A KD*, lentiviral shRNA knockdown of the *HIF2A*; CL, lentiviral shRNA against luciferase as a control. p-values are shown for each comparison.

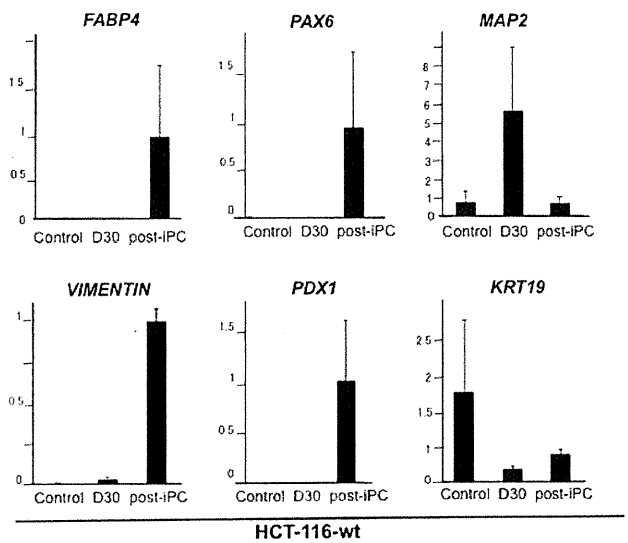

Figure 5. Multi-differentiation potential of iPC cells after reprogramming. After generating iPC cells from wt HCT116 cells in hypoxia (5% O_2), the expression levels of *FABP4, PAX6, MAP2, VIMENTIN, PDX1* and *KRT19* were analysed by qRT-PCR on day 30 (iPC; D30) or after subsequent differentiation-induction culture for 20 days (post-iPC).

HIF2A-P405A/P531A mutants, but not wild-type *HIF2A*, increased reprogramming efficiency in normoxia (4.8-times, p<0.05, Fig. 4), whereas the introduction of *HIF1A-P402A/P564A* mutants, but not wild-type *HIF1A*, increased reprogramming efficiency (2.7-times, p<0.05, Fig. 4).

In hypoxia, the expression of Tra-1-60 was increased regardless of whether wild-type or mutant *HIF1A* and *HIF2A* were co-transfected, indicating that hypoxia attenuated the effect of mutations in Hif proteins and that the Hif pathway plays a role in the increased reprogramming efficiency of cancer cells. To confirm these indications, we performed a knockdown experiment. The lentiviral shRNA transduction system indicated that knockdown lasting for at least 5 days resulted in reduced generation of Tra-1-60$^+$ cells in hypoxia. In other words, reprogramming efficiency was decreased after *HIF2A* knockdown (0.5-times, p<0.05) and *HIF1A* knockdown (0.75-times, p<0.05), but the knockdown effect was not detected in normoxia, supporting the notion that the Hif pathway plays a role in the efficiency of iPC cell generation in hypoxia. This suggests that the effect of hypoxia can be explained at least partially by the activation of the Hif2a pathway, and increased expressions in hypoxia can be explained by the activation of the Hif pathway, indicating that it is involved in the regulation of iPC cell generation.

Multi-differentiation potential of iPC cells. To assess the multi-differentiation potential of iPC cells, induced cells were subjected to *in vitro* induction of differentiation. Established iPC cells in ES culture medium were transferred to DMEM with 10% FBS (DMEM does not support growth of cells in an undifferentiated state), grown for 20 days to elicit differentiation (post-iPC cells) and their gene expression was then studied by qRT-PCR. The expression of *PDX1* (a transcription factor involved in pancreatic development), *VIMENTIN* (a mesenchymal marker) and *PAX6* (an ectoderm marker) markedly increased in post-iPC cells derived from wt HCT116 (Fig. 5) and HCT116 p53 null iPC cells (data not shown). The *MAP2* expression in post-iPC cells decreased, but remained detectable in wt HCT116 (Fig. 5) and HCT116 p53 null iPC cells (data not shown), although the expression was relatively high in wt HCT116 cells on day 30. Induction of a-Sma (muscle), Gfap (ectoderm), Vimentin, Keratin 19 (epithelial) and Tubb3 (ectoderm) proteins was confirmed by immunocytochemical staining with specific antibodies (data not shown). The data indicate that the four defined factor-induced reprogramming resulted in multi-differentiation potential in cancer cells. Next, a proliferation assay showed that cell growth was significantly

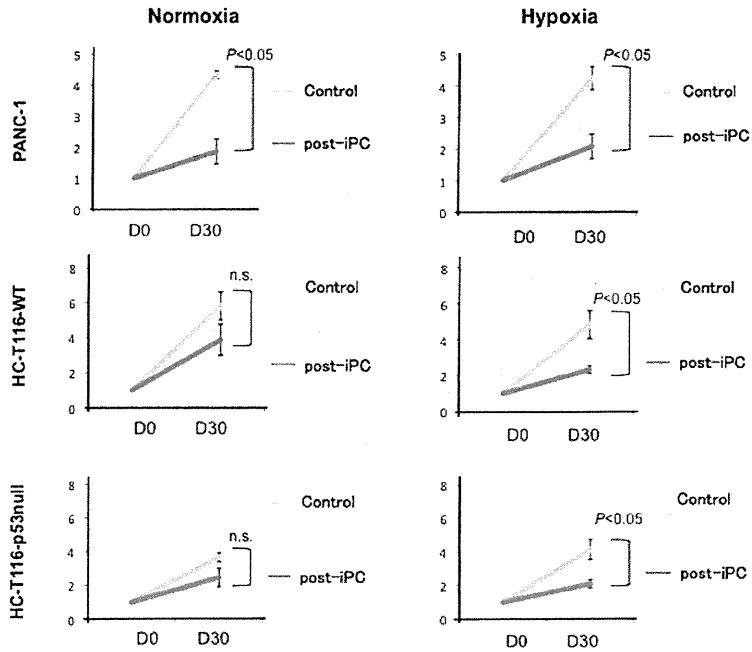

Figure 6. iPC cell proliferation assay. Control parental and iPC cells were derived from wt HCT116, HCT116 p53 null and PANC-1 cells in normoxia or hypoxia and subjected to a proliferation assay. Differences with $p<0.05$ were considered statistically significant.

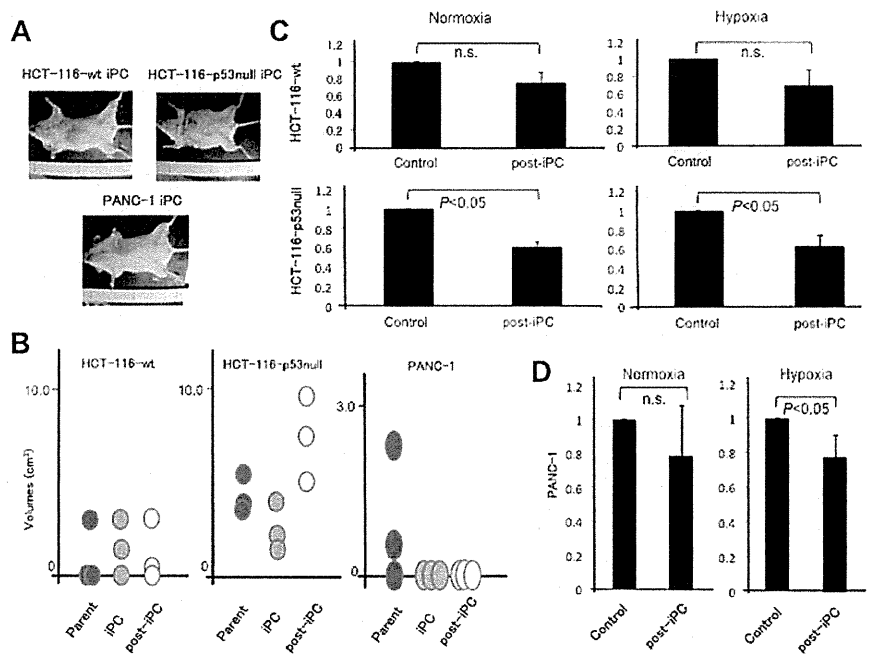

Figure 7. Tumourigenicity and invasion assay of iPC cells. (A and B) Tumourigenicity of parental wt HCT116, HCT116 p53 null and PANC-1 cells and the iPC and post-iPC cells derived from them. (C) Invasion assay of iPC cells derived from wt HCT116 and HCT116 p53 null cells in normoxia and hypoxia. (D) Invasion assay of PANC-1 iPC cells induced in normoxia and hypoxia. Differences with $p<0.05$ were considered statistically significant.

reduced in post-iPC cells derived from PANC-1 iPC cells, but not parental PANC-1 cells cultured in the same DMEM with 10% FBS, in both normoxia and hypoxia ($p<0.05$, Fig. 6). Cell growth was also significantly reduced in wt HCT116 and HCT116 p53 null cells induced in hypoxia ($p<0.05$) and, to a lesser extent, in normoxia (not significant; Fig. 6). The data suggested that reprogramming induced a distinct phenotype from parental cancer cells efficiently in hypoxia.

Tumourigenicity and invasion of iPC cells. iPC cells were inoculated into NOD/SCID mice and tumour formation was observed. The tumourigenicity of iPC and post-iPC cells derived from PANC-1 cells was reduced compared to that of parental PANC-1 cells (Fig. 7A and B). The tumourigenicity of iPC and post-iPC cells derived from wt HCT116 cells was comparable to that of parental cells. The tumourigenicity of iPC cells derived from HCT116 p53 null cells was also comparable with that of

parental HCT116 p53 null cells; however, post-iPC cells derived from HCT116 p53 null cells showed increased tumourigenicity. *In vitro* invasion assay indicated that tumourigenicity was reduced in iPC cells derived from hypoxia condition and, to a lesser extent, normoxia condition in both wt HCT116 and HCT116 p53 null cells (Fig. 7C), whereas in iPC cells derived from PANC-1 cells the reduction was greater in hypoxia than in normoxia (Fig. 7D). Thus, the present study indicates that induction of iPC cells in hypoxia could cause an enhanced reduction *in vitro*, while *in vivo* growth in *TP53*-deficient background might elicit aggressive transformation and a higher level of tumourigenicity.

Discussion

Tumours can originate from stem or progenitor cells and epigenetic alterations are involved in cellular differentiation as in *BCR/ABL* translocation-positive haematopoietic stem cells in chronic myelogenous leukaemia and Lgr5-positive stem cells in CRC (1-3). This suggests that possible corrections of the differentiation program, reversion of aggressive phenotypes or induction of apoptosis in cancer cells may be an ideal therapeutic approach. Reprogramming induction of differentiated cells by transfection of defined transcription factors considerably modifies the epigenetic machinery, but genetic alterations in cancer cannot, in principle, be corrected by the introduction of defined transcription factors. Cancer cells generally harbour genetic instability and the extent to which epigenetic modifications associated with reprogramming can modulate the biological behaviour of tumour cells remains debatable. The present study suggests that the remaining p53 allele in wt HCT116 cancer cells is involved in reprogramming regulation and that its deficiency may accelerate the reprogramming of cancer cells. Since the p53 pathway is altered in ~50% of cancer cells, such cells may be susceptible to reprogramming induction. Furthermore, the present data indicate that hypoxia enhances the reprogramming induction. Considering that cancer metabolism is adaptive to hypoxia glycolysis and that a significant fraction of cancer cells, including cancer stem cells, can presumably survive in hypoxia or in a hypoxic niche, at least two pathways, the Hif and p53 pathways, may be targeted to regulate reprogramming therapy for cancer.

The tumourigenicity assay of HCT116 p53 null cells indicated that post-iPC cells exhibited a high level of tumour formation *in vivo*, whereas an *in vitro* study demonstrated that post-iPC cells derived from HCT116 p53 null cells exhibited reduced invasive activity and a lower cell proliferation rate than control cells. Hypoxia elicited the reprogramming suggesting that the microenvironment of tumour tissues, such as vascularisation *in vivo*, might affect tumour activation and that tumour activation is not a cell-autonomous mechanism. The p53 protein has been shown to limit angiogenesis, at least partly, by interfering with the central regulators of hypoxia that mediate angiogenesis (reviewed in ref. 18). Tumours with inactivated tumour suppressor p53 function, approximately half of all tumours, appear more vascularised, are often more aggressive and are correlated with poor post-treatment prognosis. Thus, the loss of functional p53 during tumourigenesis represents an essential step in the switch in hypoxia to an angiogenic phenotype that characterises aggressive tumours (18). To inhibit malignant transformation observed in the reprogrammed *TP53*-deficient cancer cells (the present study) and in other cancer cells with gain-of-function mutations such as $TP53^{R175H}$ and $KRAS^{G12D}$ (19), we suggest that the combination of anti-angiogenic therapy and therapies targeting *TP53* deficiency may be beneficial. For example, anti-vascular endothelial growth factor receptor antibodies may suppress the deleterious effect of *TP53*-deficient reprogramming. We speculate that, although *TP53* overlapped with the hypoxia pathway, *TP53* may play a critical role in the surveillance of the malignant phenotype or deleterious mutations in reprogrammed cancer cells.

Our results suggest a specific target for reprogramming in the hypoxia pathway. The expression of Hif2α is cell-type specific and its biological role is distinct from that of Hif1α. While Hif1α is ubiquitously expressed, Hif2α is more prominently detected in vascular endothelial cells during embryonic development and is indeed an upstream regulator of *OCT3/4* (15). Furthermore, in addition to being present in endothelial cells, *HIF2α* mRNA has been detected in kidney fibroblasts, liver hepatocytes, epithelial cells of the intestinal lumen, pancreatic interstitial cells and other interstitial cells (20,21). In this study, the effect of introducing ES-like genes in gastrointestinal cancer cells may have been enhanced by hydroxylation-defective mutation of *HIF2α* and, to a lesser extent, *HIF1α*, suggesting that cell type-specific modifications involving the use of different Hif subunits could be a reliable method of fine-tuning reprogramming efficiency. To the best of our knowledge, this is the first report demonstrating involvement of the Hif family in reprogramming and iPC cell generation.

Acknowledgements

We thank Dr Bert Vogelstein (Johns Hopkins University, Baltimore, MD) for providing *TP53*-deficient cell lines. This work was partly supported by a grant from the Core Research for Evolutional Science and Technology (CREST) (H.I., M.M.), a Grant-in-Aid for Scientific Research on Priority Areas (M.M.), a Grant-in-Aid for Scientific Research from the Ministry of Education, Culture, Sports, Science and Technology (H.I., M.M.), a Grant-in-Aid for the 3rd Comprehensive 10-year Strategy for Cancer Control Ministry of Health, Labour and Welfare (H.I., M.M.), a grant from the Tokyo Biochemical Research Foundation (M.M.) and a grant from the Princess Takamatsu Cancer Research Fund, Japan (H.I.).

References

1. Tenen DG: Disruption of differentiation in human cancer: AML shows the way. Nat Rev Cancer 3: 89-101, 2003.
2. Chen J, Odenike O and Rowley JD: Leukaemogenesis: more than mutant genes. Nat Rev Cancer 10: 23-36, 2010.
3. Markowitz SD and Bertagnolli MM: Molecular origins of cancer: Molecular basis of colorectal cancer. N Engl J Med 361: 2449-2460, 2009.
4. Jones PA and Baylin SB: The fundamental role of epigenetic events in cancer. Nat Rev Genet 3: 415-428, 2002.
5. Piekarz RL and Bates SE: Epigenetic modifiers: basic understanding and clinical development. Clin Cancer Res 15: 3918-3926, 2009.
6. Takahashi K and Yamanaka S: Induction of pluripotent stem cells from mouse embryonic and adult fibroblast cultures by defined factors. Cell 126: 663-676, 2006.
7. Yamanaka S: Elite and stochastic models for induced pluripotent stem cell generation. Nature 460: 49-52, 2009.

8. Miyoshi N, Ishii H, Nagai K, *et al*: Defined factors induce reprogramming of gastrointestinal cancer cells. Proc Natl Acad Sci USA 107: 40-45, 2010.
9. Gil J and Peters G: Regulation of the INK4b-ARF-INK4a tumour suppressor locus: all for one or one for all. Nat Rev Mol Cell Biol 7: 667-677 2006.
10. Zhao Y, Yin X, Qin H, *et al*: Two supporting factors greatly improve the efficiency of human iPSC generation. Cell Stem Cell 3: 475-479, 2008.
11. Kawamura T, Suzuki J, Wang YV, *et al*: Linking the p53 tumour suppressor pathway to somatic cell reprogramming. Nature 460: 1140-1144, 2009.
12. Hong H, Takahashi K, Ichisaka T, *et al*: Suppression of induced pluripotent stem cell generation by the p53-p21 pathway. Nature 460: 1132-1135, 2009.
13. Yoshida Y, Takahashi K, Okita K, Ichisaka T and Yamanaka S: Hypoxia enhances the generation of induced pluripotent stem cells. Cell Stem Cell 5: 237-241, 2009.
14. Yeung SJ, Pan J and Lee MH: Roles of p53, MYC and HIF-1 in regulating glycolysis - the seventh hallmark of cancer. Cell Mol Life Sci 65: 3981-3999, 2008.
15. Poon E, Harris AL and Ashcroft M: Targeting the hypoxia-inducible factor (HIF) pathway in cancer. Expert Rev Mol Med 11: e26, 2009.
16. Ben-Porath I, Thomson MW, Carey VJ, Ge R, Bell GW, Regev A and Weinberg RA: An embryonic stem cell-like gene expression signature in poorly differentiated aggressive human tumors. Nat Genet 40: 499-507, 2008.
17. Takahashi K, Tanabe K, Ohnuki M, Narita M, Ichisaka T, Tomoda K and Yamanaka S: Induction of pluripotent stem cells from adult human fibroblasts by defined factors. Cell 131: 861-872, 2007.
18. Teodoro JG, Evans SK and Green MR: Inhibition of tumor angiogenesis by p53: a new role for the guardian of the genome. J Mol Med 85: 1175-1186, 2007.
19. Nagai K, Ishii H, Miyoshi N, *et al*: Long-term culture following ES-like gene-induced reprogramming elicits an aggressive phenotype in mutated cholangiocellular carcinoma cells. Biochem Biophysic Res Commun 395: 258-263, 2010.
20. Rosenberger C, Mandriota S, Jürgensen JS, *et al*: Expression of hypoxia-inducible factor-1alpha and -2alpha in hypoxic and ischemic rat kidneys. J Am Soc Nephrol 13: 1721-1732, 2002.
21. Wiesener MS, Jürgensen, JS, Rosenberger C, *et al*: Widespread hypoxia-inducible expression of HIF-2alpha in distinct cell populations of different organs. FASEB J 17: 271-273, 2003.

Biomaterials 33 (2012) 2770–2779

Contents lists available at SciVerse ScienceDirect

Biomaterials

journal homepage: www.elsevier.com/locate/biomaterials

Enhanced stability and gene silencing ability of siRNA-loaded polyion complexes formulated from polyaspartamide derivatives with a repetitive array of amino groups in the side chain

Tomoya Suma [a], Kanjiro Miyata [b], Takehiko Ishii [a], Satoshi Uchida [b], Hirokuni Uchida [a], Keiji Itaka [b], Nobuhiro Nishiyama [b], Kazunori Kataoka [a,b,c,d,*]

[a] Department of Bioengineering, Graduate School of Engineering, The University of Tokyo, 7-3-1 Hongo, Bunkyo-ku, Tokyo 113-8656, Japan
[b] Center for Disease Biology and Integrative Medicine, Graduate School of Medicine, The University of Tokyo, 7-3-1 Hongo, Bunkyo-ku, Tokyo 113-0033, Japan
[c] Department of Materials Engineering, Graduate School of Engineering, The University of Tokyo, 7-3-1 Hongo, Bunkyo-ku, Tokyo 113-8656, Japan
[d] Center for NanoBio Integration, The University of Tokyo, 7-3-1 Hongo, Bunkyo-ku, Tokyo 113-8656, Japan

ARTICLE INFO

Article history:
Received 12 October 2011
Accepted 9 December 2011
Available online 24 December 2011

Keywords:
siRNA
Poly(amino acid)
Polyion complex
Charge density
Endosomal escape

ABSTRACT

The delivery of siRNA therapeutics owes its success to the development of carrier systems with high efficacy and minimum toxicity. Here, cationic polyaspartamide derivatives with a regulated number and spacing of positively charged amino groups in the side chain were prepared from a single platform polymer of poly(β-benzyl L-aspartate) to assess their availability as siRNA carriers through polyion complex (PIC) formation. These polymers have 1,2-diaminoethane, 1,3-diaminopropane, and *N,N'*-bis(2-aminoethyl)-1,2-diaminoethane moieties in the side chain, and are termed as PAsp(DET), PAsp(DPT), and PAsp(TEP), respectively. siRNA-loaded PICs stable in serum-containing media were formed from PAsp(TEP) and PAsp(DPT) with two positive charges in the side chain at pH 7.4, whereas no such stable PIC was obtained from PAsp(DET) with only a single charge in the side chain, suggesting facilitated multivalent interactions with siRNA molecules to increase the PIC stability. The PAsp(DPT) and PAsp(TEP) PICs stable in the serum-containing media underwent an appreciably enhanced uptake into cultured cells through endocytosis, and subsequently exerted effective endosomal escape for the significant silencing of target gene expression. Notably, PAsp(TEP) PIC displayed negligible cytotoxicity in sharp contrast to the highly toxic feature of PAsp(DPT) PIC. This cytotoxicity is apparently correlated with the minimal damage to the cytoplasmic membrane of cells exposed to PAsp(TEP) at pH 7.4 evidenced from the fluorescent dye (YO-PRO-1) permeation assay. There was, in turn, a significant increase in YO-PRO-1 permeability at endosomal pH of 5.5 for PAsp(TEP)-exposed cells, indicating that PAsp(TEP) exerts membrane damage in a pH-selective manner, and eventually facilitates the translocation of siRNA-loaded PIC from the acidic endosomal compartment into the cytoplasm for effective gene silencing without any severe toxicity at physiological conditions. This acidic pH modulated enhancement in membrane damage of PAsp(TEP) may be explained by an increased protonation of the arrayed amino groups in the side chain that strongly perturb the endosomal membrane integrity. Eventually, PAsp(TEP) with a side chain array of pH-sensitive amino groups was demonstrated to be a promising component for constructing siRNA carriers exerting effective gene silencing in a less toxic context.

1. Introduction

Small interfering RNA (siRNA) enables the target-specific gene silencing through RNA interference (RNAi) machinery and has been intensely desired as a pharmaceutical agent for the treatment of various intractable diseases, such as cancers, viral infections, and genetic disorders [1]. However, siRNA has the inherent problem of poor bioavailability, such as the rapid decomposition in the body and inefficient cellular internalization. Thus, development of safe and effective delivery systems for siRNA is a current challenge for siRNA-based therapies.

Polyion complexes (PICs) formed from electrostatic interaction of polycations and anionic oligonucleotides, including siRNA, can protect oligonucleotides from enzymatic degradation and facilitate

* Corresponding author. Department of Materials Engineering, Graduate School of Engineering, The University of Tokyo, 7-3-1 Hongo, Bunkyo-ku, Tokyo 113-8656, Japan. Tel.: +81 35841 7138; fax: +81 3 5841 7139.
E-mail address: kataoka@bmw.t.u-tokyo.ac.jp (K. Kataoka).

0142-9612/$ – see front matter © 2011 Elsevier Ltd. All rights reserved.
doi:10.1016/j.biomaterials.2011.12.022

their cellular uptake. These PICs present a promising candidate for oligonucleotide carriers [2–5]. The most widely studied polycations in this regard are polyethylenimine (PEI) and its derivatives, which have low pKa amino groups contributing to a facilitated endosomal escape of PICs through the so-called proton sponge effect [6,7]. Although several studies have demonstrated significant gene silencing with siRNA-loaded PICs prepared from PEI derivatives [8–10], their cytotoxic effect is frequently a concern for clinical applications [11–13]. Accordingly, polycations showing highly efficient endosomal escape and minimal cytotoxicity in clinical settings are required for the practical formulation of siRNA-loaded PICs.

In the previous study, we reported that a polyaspartamide derivative bearing a 1,2-diaminoethane unit in the side chain (PAsp(DET)) (Fig. 1) exerted efficient and low toxic translocation of its PIC with plasmid DNA (pDNA) from the endosomal compartment into the cytoplasm through pH-selective membrane disruption [14–16]. The 1,2-diaminoethane unit in the side chain of PAsp(DET) changed from a mono-protonated state to di-protonated state responding to the pH drop in the endosomal compartment, which facilitated the interaction of PAsp(DET) with the endosomal membrane. Eventually, pDNA/PAsp(DET) PIC achieved appreciable *in vivo* transfection efficiency to show a therapeutic outcome in diseased animal models [17–20]. Nevertheless, the use of PAsp(DET) in siRNA transfection resulted in no significant efficacy because of the poor stability of siRNA/PAsp(DET) PIC in serum-containing media [21,22], suggesting that the substantially decreased number of anionic charges of siRNA compared to pDNA might reduce the association force in PIC formation with PAsp(DET). Here, we report that this stability issue of siRNA-loaded PIC was overcome by constructing a repetitive array of aminoethylene units in the side chain of the polycation to exert multivalent electrostatic interactions with siRNA, retaining both endosomal escaping functions and tolerability in serum-containing medium. Furthermore, by tuning the spacer length between repeating amine units, the toxicity issue can also be managed to construct the siRNA-loaded PIC with well-balanced properties of highly specific gene silencing potential and appreciably low cytotoxicity.

2. Materials and methods

2.1. Materials

β-Benzyl L-aspartate *N*-carboxy anhydride (BLA-NCA) was purchased from Chuo Kaseihin Co., Inc. (Tokyo, Japan). *N,N*-Dimethylformamide (DMF), dichloromethane (DCM), *n*-butylamine, diethylenetriamine (DET), tetraethylenepenatamine (TEP), dipropylenetriamine (DPT), and *N*-methyl-2-pyrrolidone (NMP) were purchased from Wako Pure Chemical Industries, Ltd. (Osaka, Japan). DMF, DCM, NMP, *n*-butylamine, DET, TEP, and DPT were distilled before use. A luciferase-expressing mouse melanoma cell line, B16F10-Luc, was purchased from Caliper LifeScience (Hopkinton, MA). Dulbecco's modified eagle's medium (DMEM) was purchased from Sigma–Aldrich Co. (St. Louis, MO). Fetal bovine serum (FBS) was purchased from Dainippon Sumitomo Pharma Co, Ltd. (Osaka, Japan). ExGen 500 was purchased from Fermentas (Ontario, Canada). Luciferase Assay System was purchased from Promega Co. (Madison, WI). All the siRNA molecules including 5′-Cy3-labeled siRNAs were synthesized by Hokkaido System Science (Hokkaido, Japan). The sequences are as follows: firefly luciferase siRNA (sense: 5′-(Cy3-) CUU ACG CUG AGU ACU UCG AdTdT-3′, antisense: 5′-UCG AAG UAC UCA GCG UAA GdTdT-3′) and scrambled siRNA (sense: 5′-UUC UCC GAA CGU GUC ACG UdTdT-3′, antisense: 5′-ACG UGA CAC GUU CGG AGA AdTdT-3′).

2.2. Synthesis of poly(β-benzyl L-aspartate) (PBLA)

PBLA was synthesized by the ring-opening polymerization of BLA-NCA initiated by *n*-butylamine as previously reported [23]. Briefly, *n*-butylamine (6 μL, 0.06 mmol) in DCM (490 μL) was added to BLA-NCA (1.40 g, 4.86 mmol) dissolved in 16.4 mL of DCM/DMF (9:1 v/v). The reaction solution was stirred for 48 h at 35 °C under an argon atmosphere. The solution was precipitated in hexane/ethyl acetate (6:4 v/v) and dried under reduced pressure overnight to obtain PBLA (888 mg, yield 77%). Size exclusion chromatography (SEC) was performed to determine the molecular weight distribution (MWD) of the obtained PBLA using a TOSOH HLC-8220 equipped with TSK gel columns (SuperAW4000 and SuperAW3000 × 2, TOSHO, Japan) and an internal refractive index (RI) detector at a flow rate of 0.3 mL min^{-1} at 40 °C. NMP with 10 mL LiBr was used as an eluent. A narrow MWD (Mw/Mn = 1.02) was confirmed from the SEC (data not shown). The degree of polymerization (DP) of the PBLA was calculated to be 92 from the peak intensity ratio of the butyl protons ($CH_3CH_2CH_2CH_2$-, δ = 0.8–1.5 ppm) at the α-chain end to the benzyl protons ($C_6H_5CH_2$-, δ = 5.1 and 7.3 ppm) at the side chain in the ^{1}H NMR spectrum (concentration: 10 mg/mL, solvent: dimethyl sulfoxide-d_6, temperature: 80 °C) (data not shown).

2.3. Synthesis of a series of cationic polyaspartamide derivatives, poly{N-[N′-(2-aminoethyl)-2-aminoethyl]aspartamide} (PAsp(DET)), poly{N-(N′-[N″-[N‴-(2-aminoethyl)-2-aminoethyl]-2-aminoethyl]-2-aminoethyl)aspartamide} (PAsp(TEP)), and poly{N-[N′-(3-aminopropyl)-3-aminopropyl]aspartamide} (PAsp(DPT))

PAsp(DET), PAsp(TEP), and PAsp(DPT) were prepared through the aminolysis reaction of PBLA with DET, TEP, and DPT, respectively, according to the previously

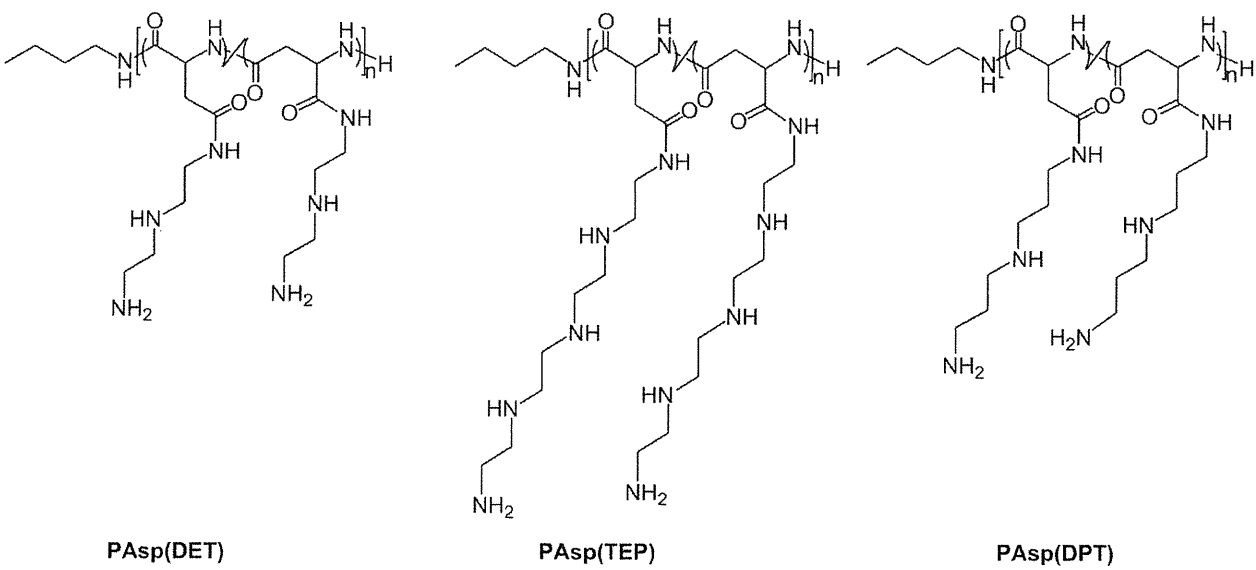

Fig. 1. Chemical structures of PAsp(DET), PAsp(TEP), and PAsp(DPT).

described method [23,24]. The typical synthetic procedure is briefly described for PAsp(DET) as follows. PBLA (DP = 92, 149 mg) was dissolved in NMP (7.5 mL) and cooled to 4 °C. DET (3.9 mL, 50 eq to benzyl groups of PBLA) was diluted with NMP (3.9 mL). The PBLA solution was added dropwise into the DET solution and the mixture stirred for 1 h at 4 °C under an argon atmosphere. Thereafter, the reaction mixture was added dropwise into a cold HCl aqueous solution (0.5 N, 21.8 mL) the temperature of which was kept below 10 °C. The polymer product was purified by dialysis against 0.01 N HCl at 4 °C for one day and then against de-ionized water at 4 °C for 4 h using a dialysis membrane with molecular weight cut off of 6000–8000 Da. The dialyzed solution was lyophilized to obtain the final product (182 mg, yield 91%) as a chloride salt form. PAsp(TEP) and PAsp(DPT) were synthesized in a similar manner; e.g., PBLA (101 mg) and TEP (4.6 mL) to obtain PAsp(TEP) (104 mg, yield 49%), and PBLA (98.9 mg) and DPT (2.8 mL) to obtain PAsp(DPT) (58.7 mg, yield 40%). Each quantitative conversion of PBLA to PAsp(DET), PAsp(TEP), and PAsp(DPT) was confirmed by the ^{1}H NMR spectra in D_2O at 80 °C (data not shown) from the peak intensity ratio of the protons of the butyl group at the α-chain end ($CH_3CH_2CH_2CH_2$-, δ = 0.8–1.5 ppm) to the ethylene protons in the aminoethylene units, i.e., PAsp(DET): $-CONH(CH_2)_2NH(CH_2)_2NH_2$, δ = 3.1–3.5 ppm; PAsp(TEP): $-CONH(CH_2)_2NH(CH_2)_2NH(CH_2)_2NH(CH_2)_2NH_2$, δ = 3.0–3.6 ppm, and to the propylene units in the 1,3-diaminopropane moieties, i.e., PAsp(DPT): $-CONH(CH_2)_3NH(CH_2)_3NH_2$, δ = 1.9–2.1 and δ = 3.1–3.3 ppm.

2.4. Potentiometric titration

PAsp(TEP) (538 mg) was dissolved in 0.1 N HCl (50 mL) containing 150 mM NaCl to adjust residual amine concentration to 100 mM. The titration was conducted with 0.1 N NaOH containing 50 mM NaCl at 37 °C, using an automatic titrator (TS-2000, Hiranuma, Kyoto, Japan). Each titrant (100 μL) was added after the stabilization of pH values (minimal interval: 30 s).

2.5. Preparation of polyion complex (PIC)

Each polyaspartamide derivative dissolved in 10 mM HEPES buffer (pH 7.4) was mixed with 15 μM siRNA solution (10 mM HEPES buffer, pH 7.4) to obtain siRNA-loaded PIC (4 μM siRNA) at the selected mixing ratio (*N/P* ratio), which was defined as the residual molar ratio of amines of the polyaspartamide derivatives to phosphates of siRNA. After the incubation for 1 h at 4 °C, the formation of PIC was determined by agarose gel electrophoresis. Each sample solution was loaded into a 1 wt% agarose gel (100 ng siRNA in 5 μl of TAE buffer (pH 7.4)) containing ethidium bromide. After electrophoresis at 100 V for 30 min, the detection was conducted using a Molecular Imager FX (BIO-RAD).

2.6. Dynamic light scattering (DLS) measurement

Size of siRNA-loaded PIC was evaluated by DLS measurements at 25 °C using a Zetasizer Nano-ZS instrument (Malvern Instruments, Malvern, UK) equipped with a He–Ne ion laser (λ = 633 nm). A scattering angle of 173° was used in all measurements. The PICs (*N/P* = 10) were prepared at 4 μM siRNA, followed by particle size measurement by DLS.

2.7. Fluorescence correlation spectroscopy (FCS) measurement

A Confocor3 module of LSM 510 (Carl Zeiss, Oberlochen, Germany), equipped with a Zeiss C-Apochromat 40× water objective, was used for FCS analysis. A He–Ne laser (543 nm) was selected for the excitation of Cy3-labeled siRNA and 560–615 nm band-pass filter was selected to filter emission. PICs prepared at 4 μM siRNA (*N/P* = 10) were diluted up to 100 nM siRNA with 10 mM HEPES buffer (pH 7.4) or DMEM containing 10% FBS. Each sample was incubated at 37 °C for the set period. Thereafter, 200 μL of samples were put into an 8-well Lab-Tek chambered borosilicate cover-glass (Nalge Nunc International, Rochester, NY) and subjected to FCS analysis (sampling time: 20 s, repeating time: 10). The measured autocorrelation curves were fitted with the Zeiss Confocor3 software to obtain diffusion times, which were then converted to the corresponding diffusion coefficients based on a reference of rhodamine6G. The corresponding diameter of the PICs was further calculated from the Stokes–Einstein equation by assuming a spherical PIC structure [25].

2.8. Luciferase gene silencing assay

B16F10-Luc cells were plated on a 24-well plate at a cell density of 10,000 cells/well in DMEM containing 10% FBS, followed by incubation for 24 h after which the medium was replaced with fresh medium. The PICs loaded with firefly luciferase or scrambled siRNA at *N/P* = 10 and 20 were applied at a concentration of 100 nM siRNA. After 48 h incubation, the medium containing siRNA-loaded PIC was removed and cells were washed with 200 μL of PBS, followed by the addition of 200 μL of cell culture lysis buffer (Promega). The expressed luciferase in the lysate was measured using a Luciferase Assay System (Promega) and a luminescence microplate reader (Mithras LB 940, Berthold technologies, Bad Wildbad, Germany). The relative luciferase expression was calculated as a ratio to the expression of non-treated cells. The results were exhibited as a mean and standard deviation of the mean obtained from four samples.

2.9. Cell viability assay

Cell viability was measured using a Cell Counting Kit-8 (Dojindo, Japan). B16F10-Luc cells were plated on a 96-well plate at a cell density of 2500 cells/well in DMEM containing 10% FBS. After incubation for 24 h, the medium was replaced with fresh medium, and siRNA-loaded PICs prepared at *N/P* = 10 and 20 were applied at a concentration of 100 nM siRNA. After 48 h incubation, the cell viability was measured following the manufacturer's protocol. The absorbance was measured using a microplate reader equipped with a band-pass filter of 450 nm (Model 680, BIO-RAD, Hercules, CA). The cell viability was determined as a percentage to the absorbance of non-treated cells. The results were expressed as a mean and standard deviation obtained from eight samples.

2.10. Flow cytometric analysis

B16F10-Luc cells were plated on a 6-well plate at a cell density of 50,000 cells/well in DMEM containing 10% FBS, followed by incubation for 24 h. PICs prepared from Cy3-labeled siRNA at *N/P* = 10 and 20 were applied to each well at a concentration of 100 nM siRNA. After 12 h of incubation, cells were washed 3 times with 500 μL of PBS, treated by trypsin-EDTA solution, and suspended in PBS. The fluorescence intensity was measured using a BD™ LSR II flow cytometer (BD Biosciences, Franklin Lakes, NJ). The results were expressed as a mean and standard deviation obtained from three samples.

2.11. Confocal laser scanning microscopic (CLSM) analysis

B16F10-Luc cells were plated on a 35 mm glass-based dish (Iwaki, Tokyo, Japan) at a density of 50,000 cells/well in DMEM containing 10% FBS followed by 24 h incubation. The old medium was replaced with fresh medium and each sample prepared from Cy3-labeled siRNA at *N/P* = 10 for PAsp(DPT) and 20 for PAsp(TEP) was applied at 100 nM siRNA. After the incubation for 24 h, the staining with LysoTracker Green (Molecular Probes, Eugene, OR) and Hoechst33342 (Dojindo, Japan) was performed, and then the CLSM imaging was conducted using the LSM 510 (Carl Zeiss, Oberlochen, Germany) equipped with a C-Apochromat 63x objective (Carl Zeiss). The excitation wavelengths were 488 nm (Ar laser) for LysoTracker Green, 543 nm (He–Ne laser) for Cy3-labeled siRNA, and 710 nm (MaiTai laser for two photon imaging) for Hoechst33342.

The intracellular distribution of Cy3-siRNA was quantitatively evaluated by calculating the colocalization ratio of Cy3-siRNA with LysoTracker Green as follows:

Colocalization ratio (%) = 100 × [yellow pixels (colocalization of Cy3 with LysoTracker)/yellow and red pixels (all the Cy3 in cells)].

The results were represented as a mean obtained from ten cells.

2.12. Membrane destabilization study

B16F10-Luc cells were plated on a 48-well plate at a cell density of 10,000 cells/well in DMEM containing 10% FBS. After 24 h of incubation, the old medium was removed. The cells were then incubated with 100 μl of PBS (pH 7.4) or 20 mM MES (pH 5.5, 150 mM NaCl) containing PAsp(DET) (5.75 μg/mL), PAsp(TEP) (4.5 μg/mL), or PAsp(DPT) (6.25 μg/mL) for 20 min at 37 °C. The concentration of each polyaspartamide derivative was adjusted to that in the gene silencing assay (*N/P* = 10). After washing cells with 1 mL of PBS, 200 μl of PBS containing YO-PRO-1 and Hoechst33342 was added to each well. After 10 min of incubation, the cells were observed with In Cell Analyzer 1000 (GE Healthcare UK Ltd., Buckinghamshire, England). The membrane destabilization activity was determined from the fluorescent intensity of YO-PRO-1 colocalizing with the Hoechst33342 signal. Approximately 3000 cells were analyzed in each well and the results represented as a mean with standard deviation obtained from three wells [26].

3. Results & discussion

3.1. Characterization of cationic polyaspartamide derivatives

Three types of cationic polyaspartamide derivatives possessing the same DP were synthesized by the quantitative aminolysis reaction to flanking benzyl ester groups of PBLA (DP = 92) [27]. Indeed, the successful preparation of PAsp(DET), PAsp(TEP), and PAsp(DPT) (Fig. 1) was confirmed by the ^{1}H NMR measurement (data not shown).

The protonated states of each polyaspartamide derivative at physiological pH of 7.4 and endosomal pH of 5.5 were estimated by the potentiometric titration in 150 mM NaCl solution at 37 °C. Each neutralization point was determined from the differential curves

Table 1
Protonation degree (α) and pKa values of each polyaspartamide derivative.

Polymer	α		pKa_1	pKa_2	pKa_3
	pH 7.4	pH 5.5			
PAsp (DPT)	0.88	0.98	9.7	8.6	
PAsp (TEP)	0.50	0.69	9.0	8.2	6.3
PAsp (DET)	0.53	0.82	9.1	6.3	

obtained from the titration curves (data not shown). The protonation degree (α) and pKa ($= pH + \log[\alpha/(1-\alpha)]$) of each polyaspartamide derivative were calculated and α/pH curves and pKa/α curves created (data not shown). Each pKa value of the flanking amine moieties in the polyaspartamide derivatives was determined from pKa/α curves (Table 1). Note that $pKa_{4,TEP}$ was not obtained here because of the incompletion of the fourth protonation of the *N,N'*-bis(2-aminoethyl)-1,2-diaminoethane unit in PAsp(TEP) even in the lower titration range of pH 1.3. Next, the α of each polyaspartamide derivative at pH 7.4 and 5.5 was determined from the α/pH curves (Table 1). From these values, the major protonated structures of PAsp(DET), PAsp(TEP), and PAsp(DPT) were estimated at pH 7.4 and 5.5 as shown in Fig. 2. PAsp(DET) and PAsp(TEP) bearing one and two 1,2-diaminoethane units, respectively, underwent substantial change in their protonation states of the side chain between pH 7.4 and 5.5: mono-protonated state at pH 7.4 and di-protonated state at pH 5.5 for PAsp(DET); and di-protonated state at pH 7.4 and tri-protonated state at pH 5.5 for PAsp(TEP). In contrast, PAsp(DPT) kept the di-protonated state at both pHs of 7.4 and 5.5. The restricted protonation of PAsp(DET) and PAsp(TEP) at pH 7.4 is reasonably explained by the electrostatic repulsion in di-protonated form of 1,2-diaminoethane unit known as the butane effect (3-bond interaction) [14]. This charge repulsive effect is diminished under 150 mM NaCl condition in 1,3-diaminopropane unit in PAsp(DPT) because of an additional methylene unit between two amino groups, leading to the fully protonation at pH 7.4.

3.2. Physicochemical characterization of siRNA-loaded PICs from cationic polyaspartamide derivatives

The cationic polyaspartamide derivatives (PAsp(DET), PAsp(TEP), and PAsp(DPT)) were applied for PIC preparation with siRNA in 10 mM HEPES buffer (pH 7.4). According to our previous results that PICs prepared at high N/P ratios (>10) showed significant gene silencing efficiency [21,22], the *N/P* = 10 and 20 were selected here for PIC preparation. Agarose gel electrophoresis of the PIC solution revealed that there were no free siRNA bands at both N/P ratios in all the samples examined, indicating the incorporation of all the siRNA molecules into the PICs. Thus, the PICs prepared at *N/P* = 10 and 20 were used for further studies.

Dynamic light scattering (DLS) analysis revealed that the size distribution of PICs (Fig. 3) was highly affected by the side chain structure of the polymers. PAsp(TEP) and PAsp(DPT) allowed the formation of monodispersed siRNA PIC with ~150 nm in size in 10 mM HEPES buffer (pH 7.4). In contrast, the PICs prepared from

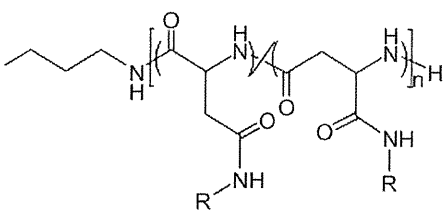

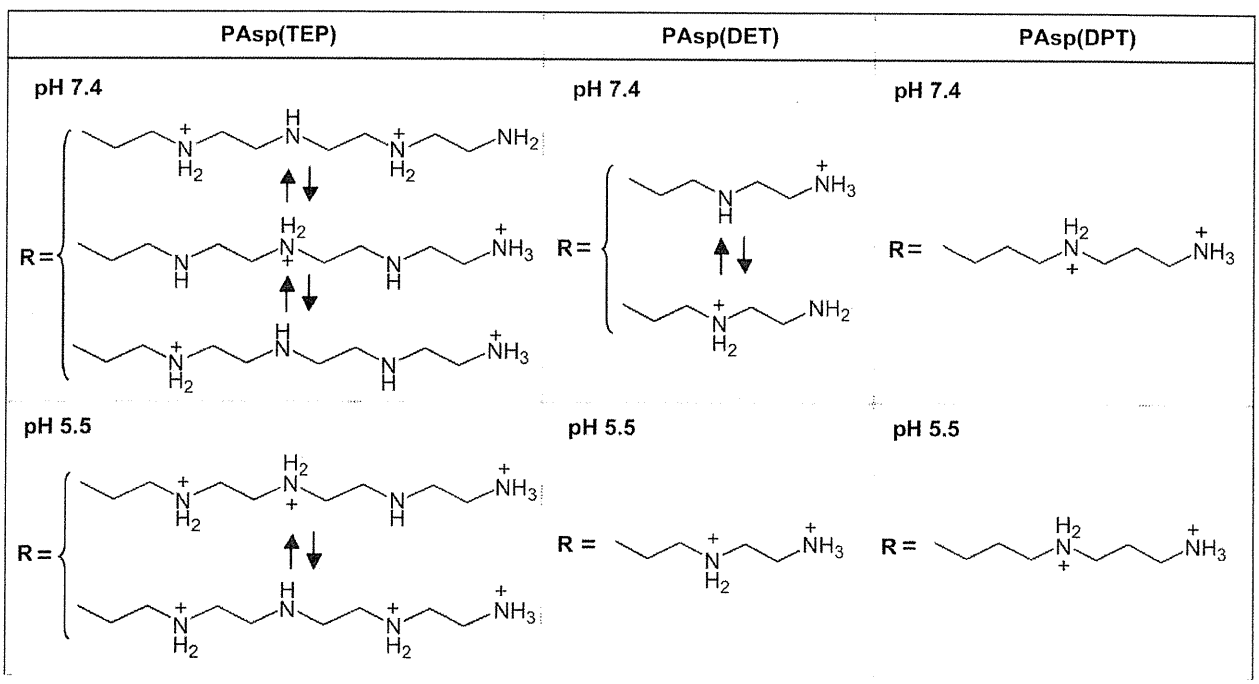

Fig. 2. Major protonated states of PAsp(DET), PAsp(TEP), and PAsp(DPT) at pH 7.4 and pH 5.5, which were estimated from the pKa values.